I THE FINAL CALIBRATION OF THE GEORGIA TECH LOW TURBULENCE WIND TUNNEL INCLUDING DYNAMIC PRESSURE AND ANGULARITY DISTRIBUTIONS AND FREE TUNNEL TURBULENCE LEVELS

II TURBULENCE STUDIES BEHIND SQUARE MESH GRIDS

III TURBULENT BOUNDARY-LAYER STUDIES ON A FLAT PLATE IN THE PRESENCE OF A ZERO LONGITUDINAL STATIC PRESSURE GRADIENT

A THESIS

Presented to

the Faculty of the Graduate Division

by

Alexander R. Ortell

In Partial Fulfillment

of the Requirements for the Degree

Master of Science in Aeronautical Engineering

Georgia Institute of Technology

August, 1957

5 A

12 T

I THE FINAL CALIBRATION OF THE GEORGIA TECH LOW TURBULENCE WIND TUNNEL INCLUDING DYNAMIC PRESSURE AND ANGULARITY DISTRIBUTIONS AND FREE TUNNEL TURBULENCE LEVELS

II TURBULENCE STUDIES BEHIND SQUARE MESH GRIDS

III TURBULENT BOUNDARY-LAYER STUDIES ON A FLAT PLATE IN THE PRESENCE OF A ZERO LONGITUDINAL STATIC PRESSURE GRADIENT

Approved by

Arnold L. Ducoffe

Robin B. Gray

Edward R. Flynt

Date Approved by Chairman September 5, 1957

In presenting this dissertation as a partial fulfillment of the requirements for an advanced degree from the Georgia Institute of Technology, I agree that the library of the institution shall make it available for inspection and circulation in accordance with its regulations governing materials of this type.

I agree that permission to copy from or to publish from, this dissertation may be granted by the professor under whose direction it was written, or, in his absence, by the Dean of the Graduate Division when such copying or publication is solely for scholarly purposes and does not involve financial gain.

It is understood that copying from, or publication of, this dissertation which involves potential financial gain will not be allowed without written permission.

Alexander R. Ortell

ACKNOWLEDGEMENTS

The author wishes to express his appreciation to Dr. Arnold L. Ducoffe for his suggestion of the subject and for his invaluable assistance during all phases of the work. Gratitude is also extended to Dr. Robin B. Gray and Mr. Edward R. Flynt for their critical review of the thesis. Mr. John M. Van Tassel (undergraduate student) is thanked for his assistance in operating the wind tunnel and recording data.

TABLE OF CONTENTS

LIST OF FIGURES

LIST OF FIGURES (CONTINUED)

NOTATION

A	line-intercept of single wire calibration curve
B	slope of single-wire calibration curve
E	voltage
e	instantaneous value of fluctuating voltage
e'	root-mean-square value of fluctuating voltage
E_1	mean voltage across wire 1 of an X-wire probe
e_1	fluctuating component of voltage due to turbulence across wire 1 of an X-wire probe
E_2	mean voltage across wire 2 of an X-wire probe
e_2	fluctuating component of voltage due to turbulence across wire 2 of an X-wire probe
E_{1_a}, E_{1_b}	mean voltage across wire 1 when X-wire probe is at an angle θ_a or θ_b to the airstream
E_{2_a}, E_{2_b}	mean voltage across wire 2 when X-wire probe is at an angle θ_a or θ_b to the airstream
e_{1_a}, e_{1_b}	fluctuating component of voltage due to turbulence across wire 1 when X-wire probe is at an angle θ_a or θ_b to the airstream
e_{2_a}, e_{2_b}	fluctuating component of voltage due to turbulence across wire 2 when X-wire probe is at an angle θ_a or θ_b to the airstream
E_d	difference in voltage between wire 1 and wire 2
ΔE_d	change in difference voltage
h_p	static pressure, inches of alcohol

NOTATION (CONTINUED)

Δh_p	static pressure at test section entrance less static pressure at any longitudinal spatial station, inches of alcohol
h_{p_z}	piezometer pressure, inches of alcohol
h_q	dynamic pressure, inches of alcohol
I	current
K_1	ratio of a change in difference voltage to the corresponding change in probe angle
L	length of wire
M	mesh size of grid, inches
R	resistance, ohms
R_{e_M}	Reynolds number, $\frac{\rho}{\mu} U_1 M$, based on mesh size
R_{e_X}	Reynolds number, $\frac{\rho}{\mu} U_1 X$, based on length, X
T	temperature of wire
T_a	temperature of ambient air
U	mean velocity in boundary layer, feet/second
U_1	mean velocity in freestream immediately outside of boundary layer, feet/second
u, v, w	X, Y, and Z components of instantaneous turbulent velocity fluctuations
$\overline{u^2}, \overline{v^2}, \overline{w^2}$	mean-square values of u, v, and w
u', v', w'	root-mean-square values of u, v, and w

NOTATION (CONTINUED)

V_i	indicated air speed in freestream, feet/second
X	longitudinal spatial position, positive upstream of test section entrance
Y	lateral spatial position, positive to the right of tunnel centerline when viewed in the upstream direction
Z	vertical spatial position, positive upward from tunnel centerline
α	resistivity of hot-wire or flow angle of attack in X-Z plane, positive upward
$\Delta\alpha$	difference in angle of attack between centerline value and value at any lateral station in a given horizontal plane
δ	boundary-layer thickness
δ^*	boundary-layer displacement thickness $\int_0^\infty \left(1 - \frac{U}{U_1}\right) dy$
θ	mean value of angle between hot-wire probe and tunnel airstream, or boundary-layer momentum thickness, $\int_0^\infty \frac{U}{U_1}\left(1 - \frac{U}{U_1}\right) dy$
μ	viscosity of air, lb sec/ft^2
ρ	mass density of air, lb sec^2/ft^4
φ	instantaneous value of fluctuating probe angle
ψ	flow angle of yaw in X-Y plane, positive left to right when viewed in the upstream direction, degrees
$\Delta\psi$	difference in angle of yaw between centerline value and the value at any lateral position in a given horizontal plane

SUMMARY

Results of the final calibration of the Georgia Tech Low Turbulence Wind Tunnel, including preliminary studies of the turbulent boundary layer on a flat plate, are presented herein. The first part of the paper gives a description of the tunnel and describes the modifications of the tunnel resulting from initial calibrations. A discussion of experimental techniques and instrumentation is then given. The final calibration included the longitudinal static pressure distribution obtained with the adjustable test section wall, dynamic pressure and angularity surveys, and freestream turbulence intensity. Measurements of the decay of turbulence behind 1 and 2 inch square mesh grids were obtained and compared with data of other facilities in order to evaluate the performance of the tunnel and hot-wire equipment. In addition, a flat plate with a roughness element near the leading edge was installed and mean velocity profiles were measured at selected longitudinal stations along the plate by means of total head and hot-wire probes. These measurements were made in a flow having a zero longitudinal static pressure gradient. Measurements of the distribution of the longitudinal turbulence component through the boundary layer at several longitudinal stations were also obtained. All calibration tests were run at a freestream velocity of 21 feet per second.

The results indicate the movable wall can be adjusted to

give a zero longitudinal static pressure gradient accurate to $\pm$ 0.002 inch of alcohol per foot of length. The dynamic pressure and angularity distributions are within acceptable limits in a central core 24 inches square except in the vicinity of the test section exit, where the open jet increases the range of deviation. The variation of the dynamic pressure is less than 0.25 per cent of the centerline value. The maximum variation from centerline values is 0.35 degrees for the angle of attack and 0.50 degrees for the angle of yaw. The free tunnel turbulence ranges from a minimum value of 0.016 per cent at the test section entrance to a maximum of 0.067 per cent for the vertical component, w', near the exit. The free tunnel turbulence in the front portion of the test section up to X = -10 feet is sufficiently low for general low turbulence work. The measurements of the decay of turbulence behind grids show good correlation with the measurements at other facilities.

The mean velocity profiles in the boundary layer of the flat plate show close agreement with the 1/7 power law. The intensity of the turbulence in the boundary layer is strongly influenced by the presence of the artificial roughness. However, downstream of the roughness element the artificial turbulence decays until the distribution of turbulence is approximately defined by a single curve independent of position along the plate.

CHAPTER I

INTRODUCTION

The airstream in a wind tunnel is never perfectly uniform and steady. Small eddies varying randomly with time in size and intensity are always present and are referred to collectively as the turbulence of the stream.

Turbulent flow is defined, in a sense, by its random fluctuations and is much too complicated a problem to be known in all its details. The solution of a turbulent motion is accomplished, if ever, by the use of statistical mechanics requiring a large amount of experimental information. This information is obtained by generating a particular turbulent motion in a wind tunnel having an extremely low freestream turbulence level and measuring the required statistical quantities by means of a hot-wire anemometer. Thus the low turbulence tunnel becomes an invaluable tool for furnishing information needed to understand the turbulence processes and to form the basis for a sound theoretical approach to them.

The use of wind tunnel data for predicting flight performance of aircraft has always been hampered by the presence of turbulence in the wind tunnel air-stream. At one time it was considered advantageous to have a high turbulence level in the wind tunnel since the effects of increased turbulence are similar to those of increased scale, which was greatly desired. However, the advent of the low-drag laminar airfoils,

which are sensitive to very low levels of turbulence, stimulated the development of low turbulence wind tunnels to provide data of increasing accuracy and applicability concerning these airfoils.

Since low turbulence wind tunnels are of such great importance in studies of turbulence effects, it seems appropriate to present the results of the calibration and the preliminary turbulence studies of the Georgia Tech Low Turbulence Wind Tunnel to illustrate its capabilities as a research tool in this field of fluid mechanics.

CHAPTER II

HISTORY OF DEVELOPMENT

General Description.—The low turbulence tunnel is of the open-circuit Eiffel type with the tunnel room serving as the return leg for the flow. This design was chosen because of space limitations. Fig. 1 shows the shape of the air passages. As will be shown later, many special features were incorporated to provide the best possible installation in the allowable space. The tunnel exit is located 128 inches, approximately 2.7 equivalent exit diameters, from the east wall. An equivalent diameter is defined as the diameter of a circular test section having the same area as the present square test section. This distance is unusually small but investigations conducted by Wharton (1) showed there is negligible effect on the static and dynamic pressure distributions (except in the vicinity of the exit) so long as the tunnel exit is located at a distance greater than one equivalent exit diameter from the wall. With the exception of the fan duct and portions of the test section the tunnel shell is built of wood. Access to the tunnel interior is provided in the diffuser, settling chamber, and test section. In order to eliminate the possibility of any turbulence due to vibration the tunnel is shock-mounted on rubber pads at all footings.

Fan Unit.--The fan is an industrial type vaneaxial fan with a diameter of 54 inches and is capable of delivering 55,000 cubic feet of air per minute against a pressure rise of 3 inches of water. The fan is powered by a 40 horsepower dc motor driven by a 50 horsepower motor-generator set. This is essentially a Ward-Leonard power system with the exception that an induction motor is used rather than the usual synchronous motor. The fan nacelle is approximately 27 inches in diameter. A fairing extends from the end of the nacelle to the entrance of the diffuser. The fairing is essentially an ogive with a blunt apex and was designed to maintain an equivalent conical diffusion angle of 7 degrees.

Wide-Angle Diffuser.--One of the unusual features of this low turbulence wind tunnel is the wide-angle diffuser which provides a large expansion of the flow without separation at the wall. This type of diffuser was necessary because of the previously mentioned space limitations. The diffuser is joined to the fan duct by a transition section which accommodates a geometry change from a round cross-section, 54 inches in diameter, to a square cross-section of the same area. The diffuser has an entrance area of 15.92 square feet and an exit area of 121 square feet. The included angle between the side walls is 77 degrees which gives an equivalent conical diffusion angle of 83 degrees. An equivalent conical diffuser is defined as a diffuser of circular cross section with the same entrance and exit areas and the same length as the square diffuser in question. Six Monel wire cloth screens (20 mesh with 0.009 inch diameter wire) are provided

to expand the flow. The screens prevent separation either by increasing the normal velocity gradient near the wall, by decreasing the pressure gradient along the wall, or by a combination of these two effects. Details on the filling effect of screens can be found in Reference 2. The positioning of these screens for the most efficient expansion without separation was determined prior to the tunnels construction by Wharton (1). The screens are installed with provisions for easy removal should cleaning or replacement be necessary.

Settling Chamber.—The settling chamber measures 11 feet square in cross section and is equipped with six 24 mesh square weave phosphor bronze damping screens which have a wire diameter of 0.0075 inches. Again provision is made for easy removal of the screens for cleaning or replacement purposes. Two extra screen frames are installed in the settling chamber should a need arise for additional screens. A honeycomb fabricated from hexagonal aluminum extrusions (8 inches long and 2 inches across flats) is installed at the entrance to the settling chamber.

Contraction.—The contraction is designed with an 11:1 contraction ratio. The shape of the contraction was derived from a fourth degree curve with the point of inflection located approximately one foot from the contraction entrance and the first and second derivatives being zero at the test section entrance. This type of curve was chosen because it gave a very gradual change in area as the test section is approached.

Test Section.--The test section is 3-1/2 feet square and 20 feet in length. The ceiling and floor are constructed of aluminum covered plywood and the south wall consists of three removable plexiglass panels. The north wall is formed by a single sheet of anodized 24 ST aluminum. The aluminum wall is movable and can be adjusted by means of five jackscrews attached to the outer surface of the wall. Thus arbitrary longitudinal pressure distributions can be induced in the test section.

Investigation to Reduce Low Frequency Surge and Improve Dynamic Pressure and Angularity Distributions.--Analysis of the initial dynamic pressure and angularity surveys in the test section indicated undesirable distributions. Also the tunnel exhibited a low frequency surge which could easily have a detrimental effect on turbulence measurements if this condition were not corrected. Investigations using pitot tubes and tufts were conducted around the tunnel entrance area, in the wide-angle diffuser, and at the tunnel exit. Two modifications to the tunnel evolved from these studies.

Before the above mentioned investigations were performed, the filtering device at the tunnel entrance consisted of 1/2 inch mesh hardware cloth supporting two layers of cheesecloth stretched across the entrance. It was noted that this filtering device pulsed excessively, and tuft studies showed the entering air possessed a great deal of rotation. Since the filter was located in high velocity region (approximately 1 foot upstream of the fan plane of rotation), this phenomenon suggested that the correspondingly high pressure drop

through the filter was causing the fan to stall. Whether or not the fan was stalled could not be accurately verified; however, a new filtering device situated in a lower velocity region was developed. This consisted of 16 vanes mounted radially around the tunnel axis spanning the distance between the tunnel entrance and the west wall. This filtering device is shown in Fig. 2 . The vanes were made of 1/4 inch plywood and measured 48 inches in length and 12 inches in width. The vanes are adjustable and their angular setting was dictated by the results of tuft studies performed on the trailing edges of the vanes. Cheesecloth wrapped around the outer perimeter provided a filter with the required low pressure drop.

The second modification was the result of tuft studies conducted along the aft portion of the nacelle. These tuft studies showed flow separation in this region. To minimize this separation an 18 x 14 mesh screen was installed approximately 8 inches upstream of the nacelle apex. This optimum position for the screen was determined using the methods and data of Schubauer and Spangenberg (2). New velocity surveys in the test section indicated that the corrective measures herein described had essentially eliminated the surge at low speeds, reduced the surge to tolerable limits at high speeds, and also improved the dynamic pressure and angularity distributions.

CHAPTER III

INSTRUMENTATION AND TECHNIQUES

Traversing Mechanism.--The traversing mechanism is designed so that longitudinal and lateral movemant of a probe can be accomplished by remote control. Two 20 foot aluminum channels, one on the floor of the test section and one on the ceiling, serve as guide rails for longitudinal movement. These channels are 6 inches wide with 2 inch legs and are mounted such that the legs face each other. The channels are connected to sleds 9 inches wide and 8 feet long which are perpendicular to the channels in a horizontal plane and form part of the floor and ceiling of the test section. The upper channel has been sprung to hold it against the ceiling along its entire length. Small rollers mounted half way between the sleds keep the channels from scoring the floor and ceiling. Electrically driven lead screws connected to the sleds provide lateral movement of the channels. In addition, a hand crank is provided to give the precise lateral movement required in positioning probes for boundary-layer investigations. The remainder of the traversing mechanism consists of a 1 inch square stainless steel strut mounted to two pieces of formica which are milled to travel along the legs of the channels. The formica slides are connected to chains driven by reversible electric motors to provide remote controlled longitudinal movement. An indicator installed on the exterior of the test section (visible in the console room)

gives the probe location longitudinally to within 1/2 inch. Another indicator in the console room gives the probe location laterally to within 1/8 inch. Limit switches are provided to protect the traversing mechanism in each travel direction. The pressure probe and hot-wire holders are attached in a manner which will give the most rigidity and least interference. Vertical positioning is accomplished by hand-turning a nut on a lead screw which is mounted parallel to the square strut. To permit the pressure and hot-wire leads to follow the probe as it is moved longitudinally, an elaborate pulley system was devised. A counterweight installed behind the pressure tubing shield assures proper tension on the leads.

Directional Pitot-Static Tube.--A directional pitot-static tube was used to measure the dynamic pressure and angularity distributions, for setting the zero longitudinal static pressure gradient, and to perform the tunnel speed calibrations. Five holes were drilled in the hemispherical head of the tube. The hole along the tube centerline measures impact pressure. Two holes in the horizontal plane, one on each side of the impact pressure hole, measure horizontal angularity and two similar holes in the vertical plane measure vertical angularity. A series of static pressure holes were located approximately eight tube diameters downstream from the impact pressure hole. Owing to slight imperfections in the construction of the instrument, it was necessary to calibrate the angularity sensitivity by placing the tube in the tunnel airstream, rotating it through known angles, and recording the change in differential pressures. Calibration curves of $\Delta p/q$ versus

flow angle were then plotted where Δp is the difference in total head due to the effect of the pitot-tube angle and q is the freestream dynamic pressure.

It should be noted that all pressures were measured with precision manometers having a reading accuracy of $\pm$ 0.001 inch of alcohol. These manometers were designed and built at Georgia Tech.

Total-Head Boundary-Layer Probe.--The total-head probe used to measure mean velocity profiles in the boundary layer was constructed from a piece of 1/16 inch inside diameter steel tubing having a 0.015 inch wall thickness. The open end of the tube was flattened to form a rectangular opening 0.125 inch by 0.015 inch. The walls were filed such that the centerline of the opening could be positioned initially 0.010 inch from the surface of the flat plate on which the turbulent boundary layer is generated. An Ames dial indicator, accurate to 0.0001 inch, was mounted on the strut of the traversing mechanism. By means of a six inch extension arm, one end of the arm in contact with the plate and the other connected to the dial gage indicator, it was possible to move the probe in known increments from the 0.010 inch reference position.

Electrical Equipment.--The electronic equipment used in conjunction with the hot-wire is a commercial unit manufactured by the Thiele-Wright Company. The equipment consists of a heater control unit, potentiometer, compensator, calibrator, amplifier, and power supply. Related equipment includes an audio-oscillator, a square-wave

generator, and a cathode-ray oscilloscope.

The heater control unit contains the current controls for heating the hot-wires and a Wheatstone bridge for measuring the resistance. The control unit also contains switching circuits so that only one amplifier is required even if more than one hot-wire is in operation. The potentiometer is used for precise measurement of voltage or current in the hot-wire. The compensator is a resistance-capacitance network which introduces the necessary compensation into the amplifier to account for thermal lag of the hot-wire. The required amount of compensation is determined by impressing a square-wave signal on the hot-wire and adjusting the compensating controls until the best possible square wave is produced on the oscilloscope screen. Calibration of the amplifier is accomplished by applying a series of known alternating voltages to the amplifier by means of the calibrator and audio-oscillator and recording the output reading for each input. The mean-square output is read on a Rawson microammeter working out of a thermo-couple circuit. The amplifier is powered by an ac power supply. The constant current to the hot-wire is provided by two banks of storage batteries supplying 72 volts to each hot-wire. Batteries were chosen because they introduce the least noise into the circuits. The noise level of the amplifier is negligible except when very low intensity turbulence measurements are made. If the hot-wire is removed from the circuit, the mean square value of the amplifier noise can be measured and subtracted from the turbulence value.

Hot-Wire Probes.--Platinum wire drawn to a diameter of 0.0001 inch by the Wollaston process was used for all hot-wire probes. A single wire probe placed perpendicularly to the flow was used to measure the turbulence intensity, u', and the mean velocity profiles in the boundary layer. X-wire probes constructed such that the wires made an angle of 30 degrees with the flow direction were used to measure v' and w'. Initial attempts to attach the wire to the supporting prongs of a u' probe consisted of etching away the silver coating and soft-soldering the wire to the tips of jeweler's broaches. This method was tedious and did not give satisfactory probe life. As a result a new method was developed for fabricating single wire probes. This consisted of soldering the unetched wire to fine sewing meedles which have had the points ground flat. Sewing needles were used instead of jeweler's broaches because of their greater rigidity. The wire was then etched in a jet of very dilute nitric acid which had silver nitrate added to precipitate any harmful chloride ions present. A pipette connected to a 2000 ml bottle created a jet of approximately 0.05 inch diameter. This produced an etched wire short enough in length to make wire length corrections unnecessary. A current of approximately 50 microamperes was passed through the etching solution to stimulate the process and insure evenly etched wires. This was done by connecting the positive terminal of a 1-1/2 volt dry cell to the probe and the negative terminal to a platinum electrode in the acid solution.

In the X arrangement the wires lie as nearly as possible in a

plane without touching. For a successful X-wire probe the wires must be perfectly matched, that is, the cold resistance of both wires must be the same. To accomplish this the etching process was monitored through one of the unused channels of the Thiele-Wright equipment. The first hot-wire was connected to the channel and to the positive terminal of the 1-1/2 volt battery and then placed in the acid jet. The etching process was continued until the wire resistance, as measured by the bridge circuit, became constant. In a similar manner the second wire was connected to the channel, care being taken not to disturb the wire from its position in the jet, and the etching process continued until the cold resistance of the second wire approached that of the first. The finished probes were checked under a microscope for proper solder joints and straightness of the etched wire. This second method produced Wollaston wire probes of the desired longevity. A schematic of this etching process is presented in Fig. 3.

The initial distance of the u' probe from the surface of the plate was determined in the following manner. An accurately machined aluminum block, 1 inch wide, 2 inches long, and 1/2 inch wide, was coated with Prussian Blue on one 1/2 x 2 inch surface. A line was scribed on the blued surface parallel to the 2 inch dimension. Gage blocks and a surface plate were utilized to accurately position this line. The block was then placed on the surface of the flat test plate such that the scribed line was vertical, faced downstream, and was parallel to the hot-wire. The adhesive force of a thin film of grease held the block to the plate. The probe was moved until the hot-wire

coincided with the reference line on the block. A transit mounted at the exit of the tunnel was used to align the hot-wire with the scribed line on the block. The dial gage indicator was also installed so that it could be viewed through the transit along with the hot-wire and reference line. The thickness of the reference line was approximately 0.0025 inch which is essentially the thickness of the Wollaston wire before etching. It was estimated that the initial probe position could be determined to within $\pm$ 0.002 inch. All succeeding probe positions were read from the dial gage indicator.

CHAPTER IV

EXPERIMENTAL TESTS

The coordinate system employed to locate stations in the test section has an origin of coordinates located at the grid slot in the entrance to the test section on the tunnel geometric centerline. The longitudinal spatial coordinate, X, is negative downstream (east) of the grid slot and positive upstream (west). The lateral coordinate, Y , is positive to the right (north) of the centerline as viewed in the upstream direction. The vertical spatial coordinate, Z, is positive upward from the centerline. The flow angle of attack, α, in the X-Z plane is positive upward. The flow angle of yaw, ψ, in the X-Y plane is positive from left to right as viewed in the upstream direction.

Longitudinal Static Pressure Gradient.--As has already been mentioned, the north wall of the test section can be adjusted to produce arbitrary static pressure gradients. The calibration of this tunnel was desired for the condition of zero longitudinal static pressure gradient. The pitot-static tube was installed on the traversing mechanism and the static pressure measured at successive one foot stations along the geometric centerline of the test section. Adjustments to the wall contour were made until the test section diverged sufficiently to offset the static pressure drop due to boundary layer growth. In this manner the condition of zero longitudinal pressure gradient was

approximated. The adjustment of the wall was made holding the fan rpm constant (constant test section velocity) at several different values of fan speed.

Speed Calibration.--The speed calibration consisted of varying the piezometer ring settings and measuring the corresponding dynamic pressure in the test section. To measure the dynamic pressure the pitot-static tube was located on the geometric centerline of the test section. Speed calibrations were made at three longitudinal stations; X = -1, -9, and -18 feet.

Dynamic Pressure and Angularity Surveys.--Dynamic pressure and flow angularity surveys were conducted with the directional pitot-static tube at an airspeed of 21 ft/sec. These surveys were made at three longitudinal stations; X = -1, -9, and -18 feet. For each longitudinal station, measurements were made at nine vertical stations and ten lateral stations. The nine vertical stations were Z = 0 (centerline), $\pm$ 3, $\pm$ 6, $\pm$ 9, and $\pm$ 12 inches. The ten lateral stations were Y = 0 (centerline), $\pm$ 3, $\pm$ 6, $\pm$ 9, $\pm$ 12, and + 15 inches. The dynamic pressure, angle of attack, and angle of yaw were measured at the stations listed.

Free Tunnel Turbulence.--The three components of turbulence were measured along the test section centerline using the hot-wire anemometer equipment. The airspeed in the test section was 21 ft/sec. The u' component of turbulence was measured using a single wire placed normal to the stream and the v' and w' components were measured using

an X-wire probe constructed such that the two wires formed an angle of 30 degrees with the airstream direction. The turbulence components were measured at nine longitudinal stations, namely, X = 0, -24, -48, -73, -96, -120, -145, -168, and -192 inches downstream of the entrance to the test section. The procedure for calibrating the single wire and X-wire probes is given in the Appendix. The method by which the root-mean-square values of turbulence are derived from the output meter reading of the compensated amplifier is also given in the Appendix.

Turbulence Behind Grids.—The measurement of turbulence behind grids has been performed many times in the past and the results correlated with isotropic turbulence theory. In order to become better acquainted with the measurement of turbulence, grids were constructed and the turbulence behind these grids measured. Comparison of the results with those of other works provided a check on the equipment. In the design of the tunnel a slot at the entrance to the test section was incorporated for the insertion of a grid. Two grids were fabricated using cold-rolled steel round bar stock. The first grid had a 2 inch square mesh using 3/8 inch diameter rods, and the second had a 1 inch square mesh using 3/16 inch diameter rods. The root-mean-square values of the turbulence components were measured behind the grids along the test section centerline. The airspeed in the test section was 21 ft/sec. For the 2 inch grid, measurements were made at $X/M \cong -10, -20, -40, -60, -80$, and -100 where M is the mesh length. For the 1 inch grid measurements were made at $X/M \cong -5, -15, -30, -45, -60, -75, -90,$

-105, -120 and -135.

Turbulent Boundary Layer on a Flat Plate With Zero Longitudinal Static Pressure Gradient.--This investigation was conducted using a flat plate 20 feet long mounted vertically in the test section and located 9 inches south of the test section centerline. The plate was 1/4 inch thick 24-ST aluminum and completely spanned the tunnel in the vertical plane. It was held in place by flush bolts which fastened the plate to 2 x 2 inch steel angles anchored to the floor and ceiling of the test section. The angles were located on the face of the plate not used as the working surface. The working surface in this case faced the adjustable north wall of the test section. The angles were anchored to the floor and ceiling by means of "dog" clamps which permitted the plate to be accurately aligned in the X-Z plane. A sharp leading edge was formed by a smooth straight taper on the back side of the working surface beginning 6 inches from the leading edge. The movable wall was adjusted to produce the condition of zero longitudinal pressure gradient. In order to insure a turbulent boundary layer on the working side of the plate, a 3 inch strip of coarse grain 36X sandpaper extending from floor to ceiling was glued to the plate. The leading edge of the sandpaper was located 3 inches downstream of the plate leading edge.

Mean velocity boundary-layer profiles were measured with the total head probe and the hot-wire anemometer. Traverses through the boundary layer were made at six longitudinal stations, namely, X = -1, -2, -5, -10, -15, and -18.7 feet, at a tunnel speed of 21 ft/sec. Measurements of the turbulence intensity, u', were made at the same time the mean velocity values were measured.

CHAPTER V

DISCUSSION OF RESULTS

Longitudinal Static Pressure Gradient.--Fig. 4 shows the longitudinal static pressure distribution along the tunnel geometric centerline after the movable wall was adjusted to give a zero pressure gradient. Two distributions are shown, one for the free tunnel at a speed of 25 ft/sec. and a second at a speed of 21 ft/sec. with the flat plate mounted in the tunnel. The ordinate, Δh_p, represents the difference in the pressure at the X = 0 station and each succeeding downstream station. In each case the data indicate that essentially a zero longitudinal static pressure gradient can be produced since the maximum observed deviations of $\pm$ 0.002 inch of alcohol are very close to the reading accuracy of the manometers.

Speed Calibration.--The results of the speed calibration are shown in Fig. 5 as a plot of piezometer pressure versus indicated airspeed. The data shown are for the longitudinal stations, X = -1, -9, and -18 feet as measured from the test section entrance. The data points for a particular piezometer setting are sufficiently close to indicate that a single curve can be used for setting the speed at any longitudinal station without introducing appreciable error. A small overall increase in velocity amounting to approximately 3 per cent occurred at the X = -18 foot station. This was believed to be due to the proximity of the east wall of the tunnel room which caused a rise in static

pressure between the wall and the tunnel exit. It was necessary to make the adjustable wall converge slightly in the region of the tunnel exit in order to maintain the desired constant static pressure. This narrowing of the air passage near the exit caused the freestream velocity to increase slightly. More detailed information on the influence of wall proximity on the flow properties at the exit of a wind tunnel can be found in Reference 1.

Dynamic Pressure Surveys.--Typical plots of dynamic pressure versus lateral position at a freestream velocity, U_1, of 21 ft/sec. are shown in Fig. 6. Dynamic pressure surveys were also made at a freestream velocity of 50 ft/sec. The surveys at 50 ft/sec. showed the variation in dynamic pressure is less than 0.25 per cent of the centerline value within a central core defined by $-18 < X$ (feet) < 0, $-12 < Y$ (inches) < 12, and $-12 < Z$ (inches) < 12. It is noted that the change in dynamic pressure from the mean at $U_1 = 21$ ft/sec. is of the order of $\pm$ 0.001 inch of alcohol which is of the same order as the sensitivity of the manometers. At $U_1 = 50$ ft/sec. the changes in dynamic pressure, h_q inches of alcohol, in the central core are of essentially the same order of magnitude as those shown in Fig. 6. However, the absolute value of the dynamic pressure is increased and hence the percentage of variation is decreased. This is paradoxical since the most uniform distribution should occur at the lower velocities. On this basis, it is argued that the variations shown in Fig. 6 are the result of insensitivity of the manometry, and that 0.25 per cent of the centerline value is the actual variation.

Angularity Surveys.--The variations from centerline values of the angle of attack, α, in the X-Z plane are shown in Fig. 7. Fig. 8 shows the variations from center line values of the angle of yaw, ψ, in the X-Y plane. Since the values of α and ψ at the centerline were used as reference or zero values, the flow angles shown in these figures are differentials and are plotted as delta values. The data for these figures were taken at a freestream velocity, U_1, of 21 ft/sec. Fig. 7 shows that the angle of attack does not vary more than $\pm$ 0.35 degrees in the central core at the X = -1 and X = -9 foot stations, but a maximum deviation of 0.50 degrees is attained at the X = -18 foot station. In Fig. 8 it is seen that the maximum variation of yaw angle from centerline values is of the order of $\pm$ 0.50 degrees except at the X = -18 foot station where the maximum deviation is -1.00 degrees. The larger values of $\Delta\psi$ at the X = -18 foot station are attributed to the converging contour of the adjustable wall at this station which causes a greater deflection of the airstream toward the center of the test section.

Free Tunnel Turbulence.--The distributions of free tunnel turbulence intensities along the geometric centerline of the test section are presented in Fig. 9. At the test section entrance, u', v', and w' are essentially the same, which indicates that the damping screens have reduced the turbulence to a sufficiently low level such that the contraction has little effect in producing a nonisotropic condition here. The intensity of each component increases progressively downstream until a maximum is reached at the tunnel exit. The vertical component, w',

exhibits the largest increase in intensity attaining a value of 0.067 per cent of freestream velocity at the X = -192 inch station. The increase in turbulence along the test section centerline is apparently due to the turbulent wakes generated by the open channels of the traversing mechanism. If it is assumed that the turbulent wakes from the channels diverge at a 7 degree angle, the intersection of these wakes occur at approximately X = -144 inches. Data points in Fig. 9 show a sharp increase in u' in the region of X = -144 inches which lends support to the wake theory. Thus a region of interaction between the turbulent channel wakes and the freestream exists along the test section centerline from the X = -12 foot station to the tunnel exit. These turbulent wakes probably also affect the free tunnel turbulence level a considerable distance upstream from the point of intersection of the wakes. This was the logic used in attributing the increase in turbulence to the channel wakes. Unfortunately, sufficient time was not available to investigate fully the effect of the channels nor was there time to determine any other causes for the increase in turbulence level. In the future these channels will be covered by a fairing to minimize the possibility of generating turbulent wakes. With the channel wakes present, the tunnel is considered acceptable for low turbulence work in the region of the test section bounded by $-10 < X$ (feet) < 0.

Turbulence Behind Grids.--The decay of the three turbulence components at various distances behind 1 and 2 inch square mesh grids is presented in Fig. 10. It is seen from Fig. 10 that most of the measurements of

$(U_1/u')^2$, $(U_1/v')^2$, and $(U_1/w')^2$ vary linearly with X/M over the range $20 < X/M < 100$. In addition, Fig. 10 shows that the condition of isotropy, $u'^2 = v'^2 = w'^2$, is closely approximated over the range of X/M values examined, although the values of $(U_1/u')^2$ for the 1 inch mesh grid and $(U_1/w')^2$ for the 2 inch mesh grid deviate from the isotropic condition as X/M exceeds 80. The tendency of $(U_1/u')^2$ to deviate from a linear decay is also exhibited in similar measurements of Batchelor and Townsend (3). Comparison is made in Fig. 11 with the data of the present tests and data of Reference 3 concerning the decay of $(U_1/u')^2$ behind 1 and 2 inch square mesh grids. The two sets of data show close agreement over the range $20 < X/M < 60$ which represents the range of X/M examined in Reference 3. The Reynolds number, R_{e_M}, based on mesh size and a freestream velocity of 21 ft/sec is 11,000 in Reference 3 for 1 inch mesh grids and 10,000 in the present tests. For the 2 inch grid data R_{e_M} is 22,100 in Reference 3 and 20,000 in the present tests.

Turbulent Boundary Layer on a Flat Plate With Zero Longitudinal Static Pressure Gradient.--Typical plots of U/U_1 versus Y are shown in Figs. 12 and 13 for a test section velocity of 21 ft/sec. These mean velocity profiles show reasonable agreement between measurements obtained with the hot-wire and those obtained by the total head probe. Fig. 14 presents a comparison with measurements obtained in the present tests and the 1/7 power law for mean velocity profiles in a turbulent boundary layer. The 1/7 power law, i.e.,

$$U/U_1 = (y/\delta)^{1/7}$$

gives a good approximation for the velocity profiles for R_{e_X} from 5×10^5 up to 10^7 (Ref. 4). The Reynolds number range for the present tests lies between 1.14×10^5 at the X = -1 foot station and 2.23×10^6 at the X = -18.7 foot station. Although the Reynolds number at X = -1 and X = -2 feet are below 5×10^5 given as the lower limit (Ref. 4), the agreement between theory and experiment shown in Fig. 14 indicates that the 1/7 power law adequately defines the velocity profiles at these two stations.

Fig. 15 shows a comparison of boundary-layer thickness, δ, boundary-layer displacement thickness, δ^*, and boundary-layer momentum thickness, θ, measured in the present tests with those given by the 1/7 power law. The boundary-layer displacement thickness and momentum thickness are defined as

$$\delta^* = \int_0^\infty \left(1 - \frac{U}{U_1}\right) dy \qquad (1)$$

$$\theta = \int_0^\infty \frac{U}{U_1}\left(1 - \frac{U}{U_1}\right) dy \qquad (2)$$

The 1/7 power law values (Ref. 4) are given as

$$\delta = \frac{0.37\,X}{(R_{e_X})^{0.2}} \qquad (3)$$

where

$$R_{e_X} = \frac{\rho}{\mu} U_1 X$$

$$\theta = 7/72\,\delta \qquad (4)$$

$$\delta^* = 1/8\,\delta \qquad (5)$$

The agreement between experiment and theory is good which was to be expected since the velocity profiles all showed good agreement with the 1/7 power law.

The variation of intensity of the longitudinal turbulence component, u'/U_1, in the boundary layer is shown in Fig. 16. From this figure it is seen that the intensity reaches its maximum close to the wall and then decreases as either the wall or outer edge of the boundary layer is approached. Fig. 16 also shows the turbulence produced by the sandpaper to be quite large at the X = -1 and X = -2 foot stations, but has decreased at the X = -5 foot station. From X = -5 to X = -18.7 feet the distributions of u' exhibit similarity and u' is essentially constant for constant y/δ. In this region the influence of the roughness has essentially disappeared.

CHAPTER VI

CONCLUSIONS

From the calibrations and turbulence measurements obtained in this investigation, the following conclusions can be drawn:

1. The movable wall of the test section can be adjusted to give a zero longitudinal static pressure gradient accurate to within $\pm$ 0.002 inch of alcohol per foot of length.
2. The deviations from centerline values of the dynamic pressure and angularity distributions are within the desired limits except in the vicinity of the test section exit where the open jet and converging contour of the adjustable wall influence the distributions.
3. The freestream turbulence intensity in the front portion of the test section up to X = -10 feet is sufficiently low for general low turbulence work.
4. The measurements of the decay of turbulence behind 1 and 2 inch square mesh grids show good agreement with measurements of other facilities. This leads to the conclusion that the present hot-wire anemometer is a reliable instrument for accurately measuring turbulent quantities.
5. The close agreement of the measured boundary-layer velocity profiles with the 1/7 power law is interpreted to mean the

existence of a fully-developed turbulent boundary layer on the flat plate.

6. The roughness element (sandpaper) mounted near the leading edge of the plate generates a region of high turbulence which diminishes rapidly in the downstream direction until a constant u' distribution forms between $X = -5$ and $X = -18.7$ feet.

CHAPTER VII

RECOMMENDATIONS

1. It is recommended that investigations be conducted to determine how accurately the adjustable wall of the test section can induce arbitrary longitudinal static pressure distributions and determine what effect this will have on the dynamic pressure and angularity distributions.
2. Thorough studies should be performed to determine exactly what effect the channels of the traversing mechanism have on the freestream turbulence intensity. If these studies show that the channels have an adverse effect, a fairing should be designed for the channels to minimize their effects.
3. If the channels are found to have a negligible effect on the freestream turbulence, other studies should be undertaken to determine why the freestream turbulence intensity increases progressively downstream.

APPENDIX

BASIC HOT-WIRE THEORY

Theory of Single Wire Probes.--The relation between the air velocity normal to a heated wire and the rate of heat loss as given by King (5) is

$$\text{heat loss} = L(T - T_a)\,(A_1 + B_1\,U^{1/2}) \qquad (1)$$

where L = length of wire

T = temperature of wire

T_a = temperature of ambient air

U = airstream velocity normal to wire

A_1, B_1 = constants

In the term, $A_1 + B_1\,U^{1/2}$, A_1 represents the heat loss due to free convection and $B_1\,U^{1/2}$ represents the forced convection heat loss. Under equilibrium conditions, the heat loss is equal to the heat supplied. A second expression for heat loss can be written as

$$\text{heat loss} = I^2\,R \qquad (2)$$

where R = resistance of wire

I = current

Pure metals possess a linear relationship between temperature and resistance so that

$$R - R_a = \alpha\,(T - T_a) \qquad (3)$$

where α = resistivity

R = resistance at temperature, T

R_a = resistance at temperature, T_a

Substitution of equations (2) and (3) into equation (1) yields

$$\frac{I^2 R}{\frac{L}{\alpha}(R - R_a)} = A_1 + B_1 U^{1/2} \qquad (4)$$

L and α are constants for a given wire and since the wires used in this investigation were operated under constant current conditions, I^2 is also a constant. All three constants may therefore be combined under A_1 and B_1 such that the following basic hot-wire equation results

$$\frac{R}{R - R_a} = A + B U^{1/2} \qquad (5)$$

This suggests a linear curve such as Fig. 17 in which $\frac{R}{R - R_a}$ is plotted versus $U_1^{1/2}$. The curve is used to determine mean velocities when the resistances, R_a and R, are known.

The procedure for determining equation (5) for a particular wire is as follows:

(1) Install the probe in the test section and measure the cold resistance, R_a.

(2) Establish a suitable heating current and hold this current constant throughout the run.

(3) Measure R at a sufficient number of freestream velocities to accurately define the curve.

When a heated wire is placed in an airstream, the fluctuating magnitude of the velocity normal to the wire induces a change in temperature and resistance and hence a change in the voltage (constant current operation) across the wire. Equation (5) is based on equilibrium conditions, but when measurements are made with an amplifier properly compensated for thermal lag of the wire, equation (5) may also be assumed to be true for instantaneous values when the velocity, U, is fluctuating. The voltage change across the wire for a given change in velocity, dE/dU, is therefore the sensitivity of the instrument for measuring velocity fluctuations. Differentiation of equation (5) yields

$$\frac{-R_a\, dR}{(R - R_a)^2} = \frac{1}{2}\, B U^{-1/2}\, dU \qquad (6)$$

Multiplication of both sides by I and use of the relations

$$E = I R \text{ and } dE = I\, dR \text{ (for constant current operation)}$$

gives

$$\frac{-R_a\, dE}{(R - R_a)^2} = \frac{1}{2}\, I B U^{-1/2}\, dU$$

or

$$dE = -\frac{(R - R_a)^2\, I B U^{-1/2}}{2 R_a}\, dU \qquad (7)$$

Replacement of the differentials dE and dU by e and U respectively to denote the instantaneous values of the fluctuating components of E and U, permits equation (7) to be written as

$$e = \frac{(R - R_a)^2 \, I \, BU^{-1/2}}{2 \, R_a} \, u \tag{8}$$

The corresponding root-mean-square values are written as

$$e' = \sqrt{\left\{ \frac{(R - R_a)^2 \, I \, BU^{-1/2}}{2 \, R_a} \right\}^2} \, u'$$

or

$$e' = \frac{(R - R_a)^2 \, I \, BU^{-1/2}}{2 \, R_a} \, u' \tag{9}$$

Solving for u' and dividing both sides by U gives

$$\frac{u'}{U} = \frac{2 \, R_a \, e'}{(R - R_a)^2 \, I \, B \sqrt{U}} \tag{10}$$

All quantities on the right of equation (10) with the exception of B, are determined at each point where u'/U is being measured. The constant, B, is found from the plot of $\frac{R}{R - R_a}$ versus $U_1^{1/2}$.

X-Wire Probe Theory.--The turbulence components, v and w, which are small compared to the mean velocity, U, result in angular changes in wind direction with negligible change in the magnitude of wind velocity. Therefore v and w components of turbulence may be measured by measuring fluctuations in wind direction. For angular measurements the X-wire probe has its two crossed wires heated by separate batteries, and the wires connected in series with such polarity that the output voltage is the difference between the voltages across the two wires.

It has been shown (6) that for small turbulence values the output voltage is relatively insensitive to changes in magnitude of the wind velocity and to angular changes perpendicular to the plane of the wires, and that angular changes in the plane of the two wires result in nearly linear changes in output voltage over a fairly large range of angles.

If a wind source completely free of turbulence were available, it is apparent that the angular sensitivity of the X-wire probe could be calibrated simply by rotating the probe through a series of known increments of angle and plotting voltage output against angular position. It remains to be shown that the probe can be calibrated in a wind tunnel having an unknown amount of turbulence.

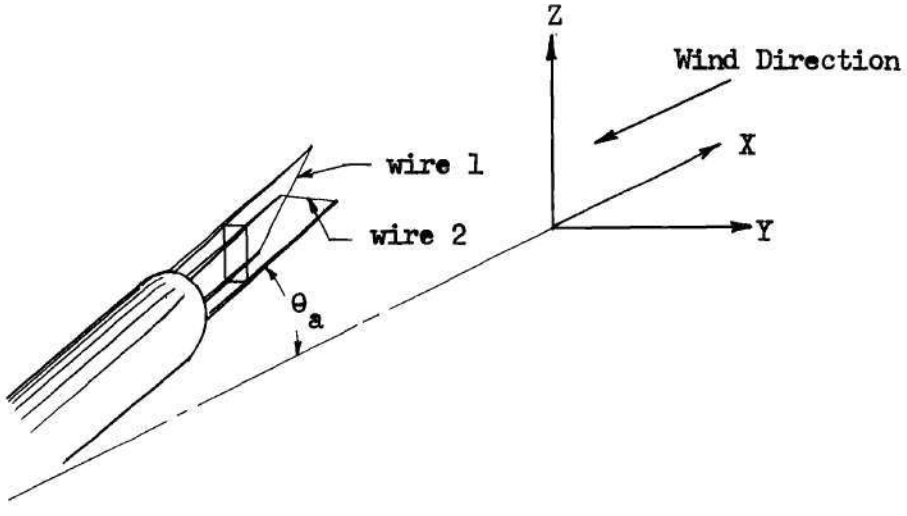

Fig. 18 X-Wire Probe

Consider the probe in Fig. 18 at an angle θ_a to the axis of the tunnel. Let

$E_{1_a} + e_{1_a}$ = voltage across wire 1 when probe is at angle θ_a

where E_{1_a} = mean voltage

e_{1_a} = fluctuating component of voltage due to turbulence

$E_{2_a} + e_{2_a}$ = voltage across wire 2 when probe is at angle θ_a

$\theta_a + \varphi_a$ = angle between probe axis and wind direction

where θ_a = angle between probe axis and mean wind direction

φ_a = fluctuation in wind direction due to turbulence

Now consider the probe to be rotated to some new angle θ_b.

$E_{1_b} + e_{1_b}$ = voltage across wire 1 when probe is at angle θ_b

$E_{2_b} + e_{2_b}$ = voltage across wire 2 when probe is at angle θ_b

$\theta_b + \varphi_b$ = angle between probe axis and wind direction

where θ_b = angle between probe axis and mean wind direction

φ_b = fluctuation in wind direction due to turbulence

The difference between the voltages across the two wires is

$$(E_{1_a} + e_{1_a}) - (E_{2_a} + e_{2_a}) \quad \text{at} \quad \theta_a$$

and

$$(E_{1_b} + e_{1_b}) - (E_{2_b} + e_{2_b}) \quad \text{at} \quad \theta_b$$

The following relation can now be written:

$$\frac{\Delta E_d}{\Delta \theta} = \frac{\left\{(E_{1_a} + e_{1_a}) - (E_{2_a} + e_{2_a})\right\} - \left\{(E_{1_b} + e_{1_b}) - (E_{2_b} + e_{2_b})\right\}}{(\theta_a + \varphi_a) - (\theta_b + \varphi_b)} \tag{11}$$

where E_d is the difference voltage obtained as the output of the two wires in series when the probe is at angle θ_a or θ_b, and ΔE_d is the change in this difference voltage, resulting from a change in angle. Taking mean values of both sides yields

$$\frac{\overline{\Delta E_d}}{\Delta \theta} = \frac{(\overline{E_{1_a}} - \overline{E_{2_a}}) - (\overline{E_{1_b}} - \overline{E_{2_b}})}{\overline{\theta_a} - \overline{\theta_b}} \tag{12}$$

The quantities e_{1_a}, e_{2_a}, e_{1_b}, e_{2_b}, φ_a, and φ_b become zero when the mean is taken, since they were defined as fluctuations about the mean. The mean-value signs may be removed from equation (12), since the remaining terms are all constants. In the actual calibration process the voltages are read by a potentiometer which is sensitive only to mean values of voltage. The change in angle, $\Delta\theta$, is a measured change in direction of the probe axis with respect to a fixed arbitrary reference axis. Since the mean wind direction is fixed with respect to the arbitrary reference axis, $\Delta\theta$ can therefore

be considered as the change in angle between the probe axis and mean wind direction.

A plot of difference voltage, E_d , versus angle, θ, shows a linear variation over a wide range of θ so that equation (12) may be written

$$\frac{\Delta E_d}{\Delta \theta} = \frac{(E_{1_a} - E_{2_a}) - (E_{1_b} - E_{2_b})}{\theta_a - \theta_b} = K_1 \qquad (13)$$

The value of K_1 , the angular sensitivity, was measured for average values of voltage and angle, but it would be the same for constant values. It would also be the same for instantaneous values, provided the instantaneous voltages were measured with an amplifier properly compensated for thermal lag of the wires, hence

$$e_1 - e_2 = \Delta E_d$$

where e_1 = instantaneous fluctuating component of voltage in wire 1

e_2 = instantaneous fluctuating component of voltage in wire 2

$$\frac{e_1 - e_2}{K_1} = \Delta E_d \frac{\Delta \theta}{\Delta E_d} = \Delta \theta \qquad (14)$$

For small values of θ such that $\tan \theta \cong \theta$,

$$\Delta \theta = \frac{v}{U} \qquad (15)$$

Combining equations (14) and (15),

$$\frac{e_1 - e_2}{K_1} = \frac{v}{U} \tag{16}$$

The corresponding root-mean-square values are

$$\frac{\sqrt{\overline{(e_1 - e_2)^2}}}{\sqrt{K_1^2}} = \frac{\sqrt{\overline{v^2}}}{\sqrt{U^2}} \tag{17}$$

Since K_1 and U are constants,

$$\frac{v'}{U} = \frac{\sqrt{\overline{(e_1 - e_2)^2}}}{K_1} \tag{18}$$

where v'/U is the fractional turbulence and $\sqrt{\overline{(e_1 - e_2)^2}}$ is determined from the calibrated output of the amplifier. If the probe is rotated 90 degrees, so that the wires lie in the X-Z plane, w' is determined,

$$\frac{w'}{U} = \frac{\sqrt{\overline{(e_1 - e_2)^2}}}{K_1} \tag{19}$$

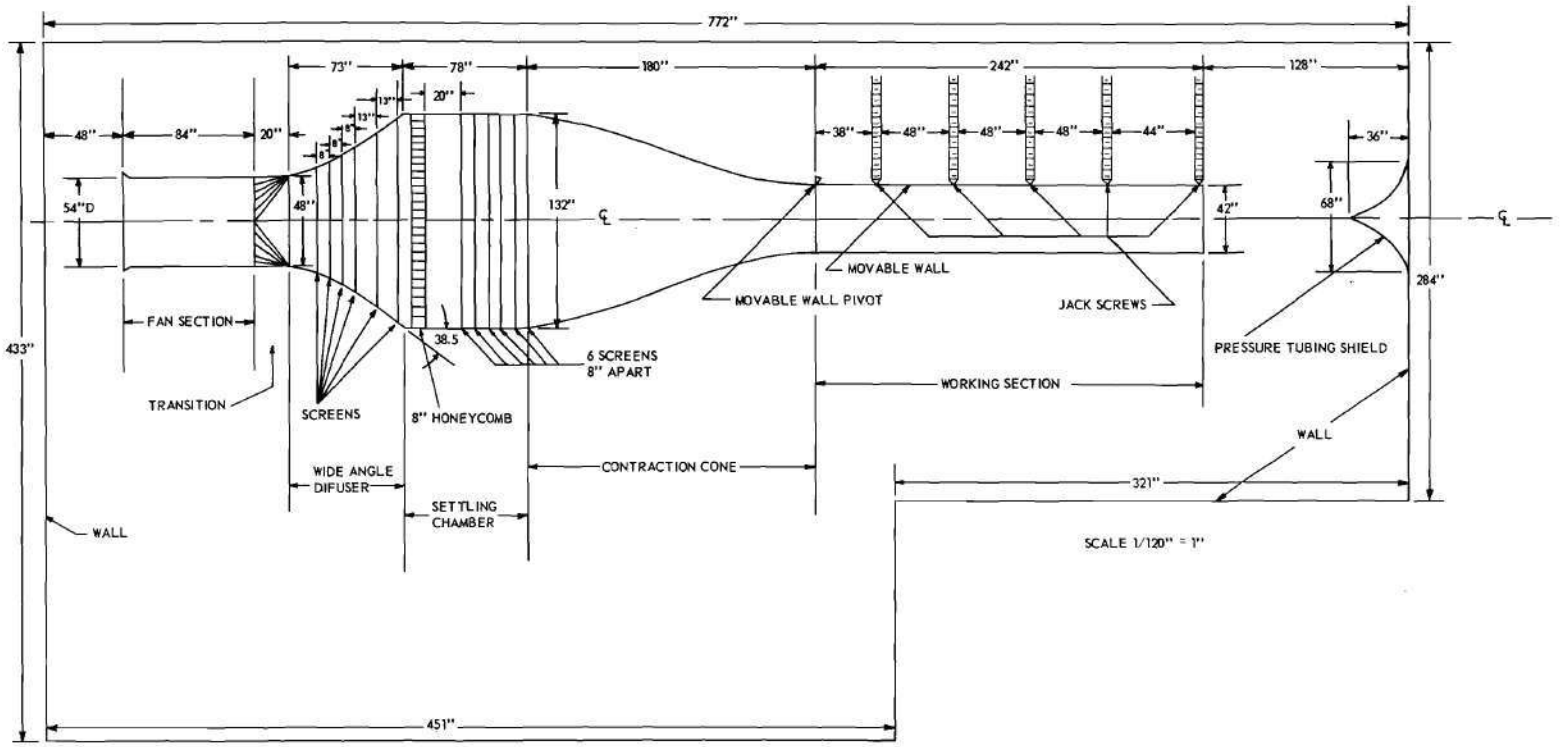

Figure 1. Schematic of Low Turbulence Wind Tunnel.

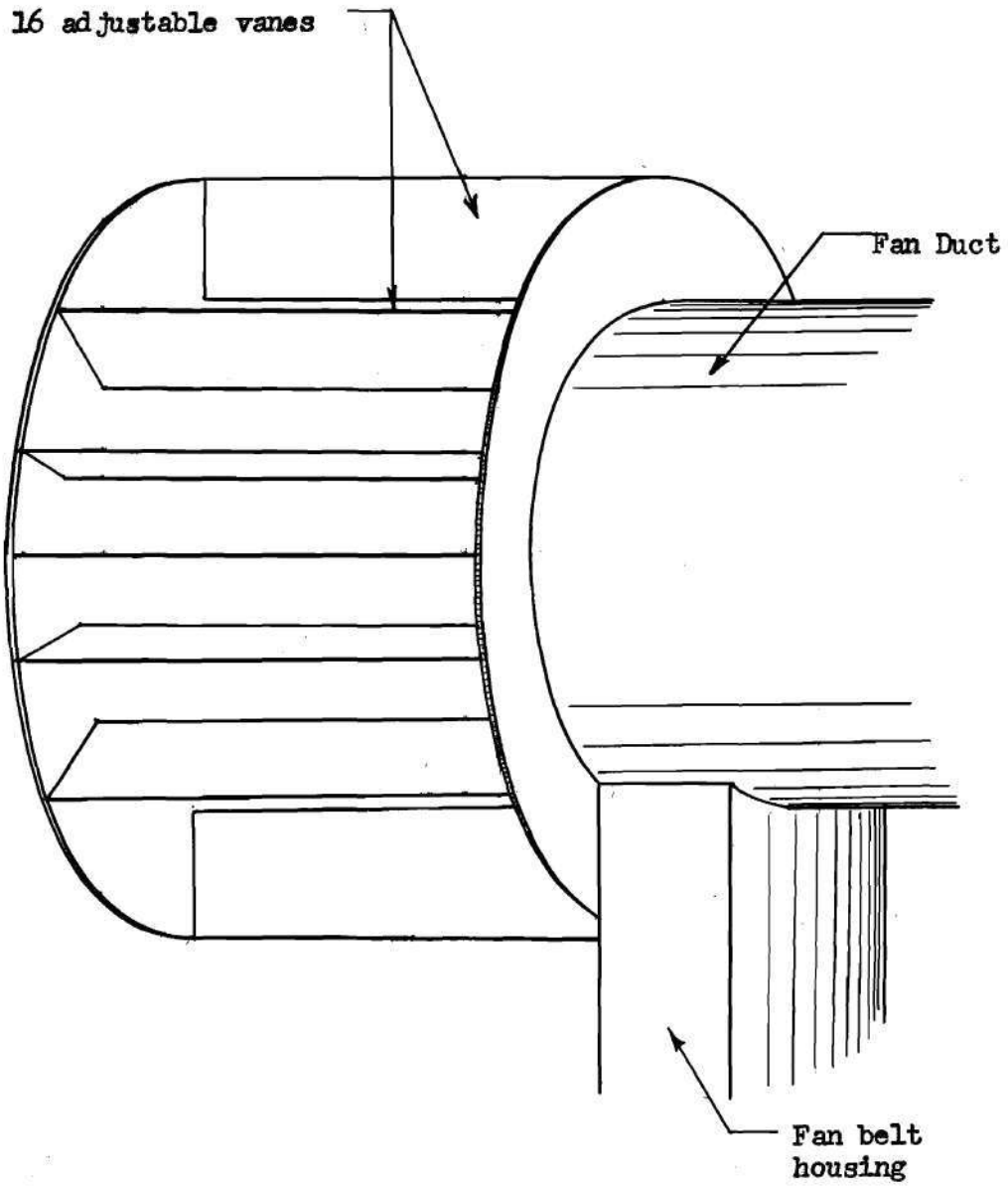

Fig. 2 Inlet Filter

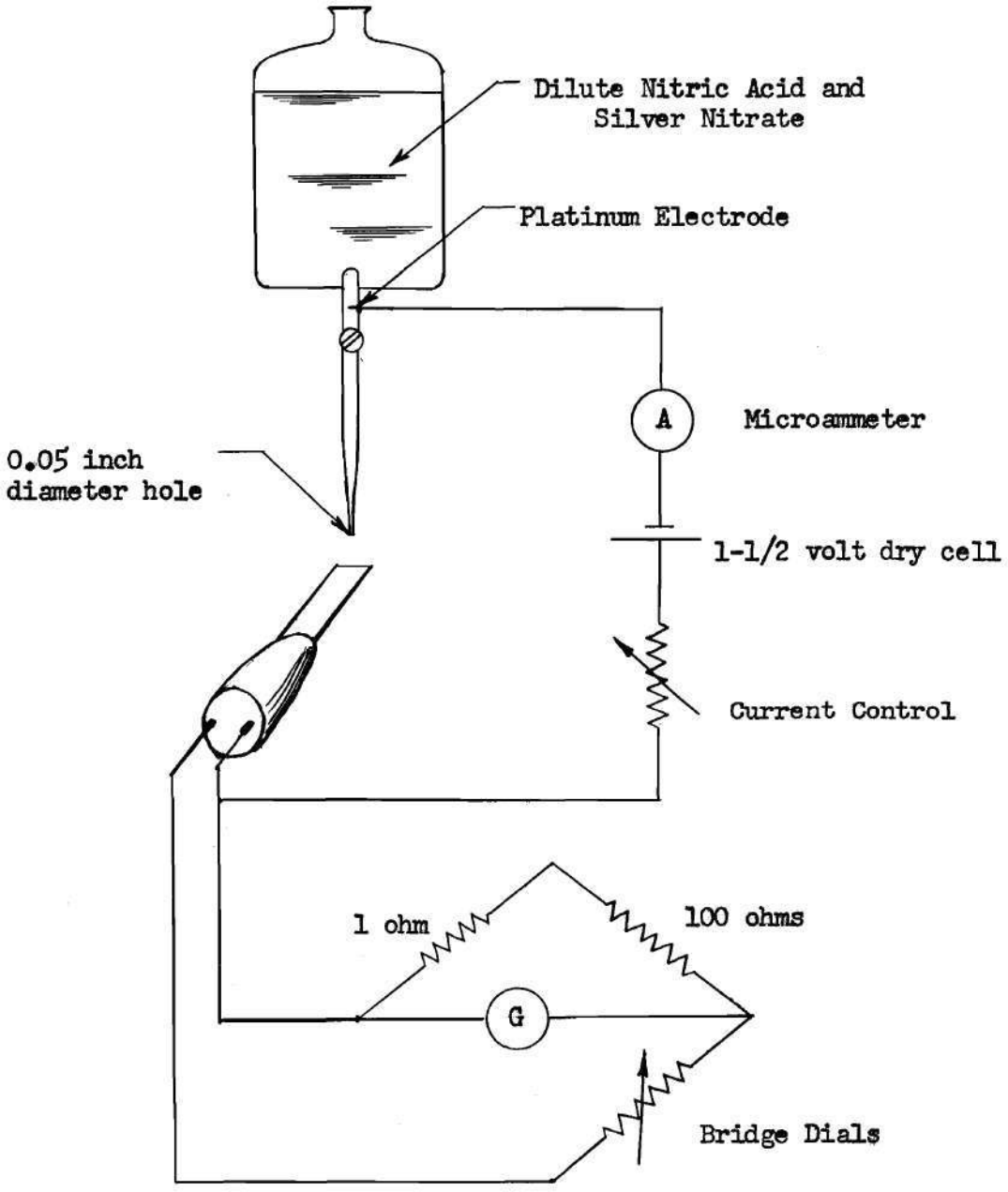

Fig. 3 Schematic of Hot-Wire Etching Process

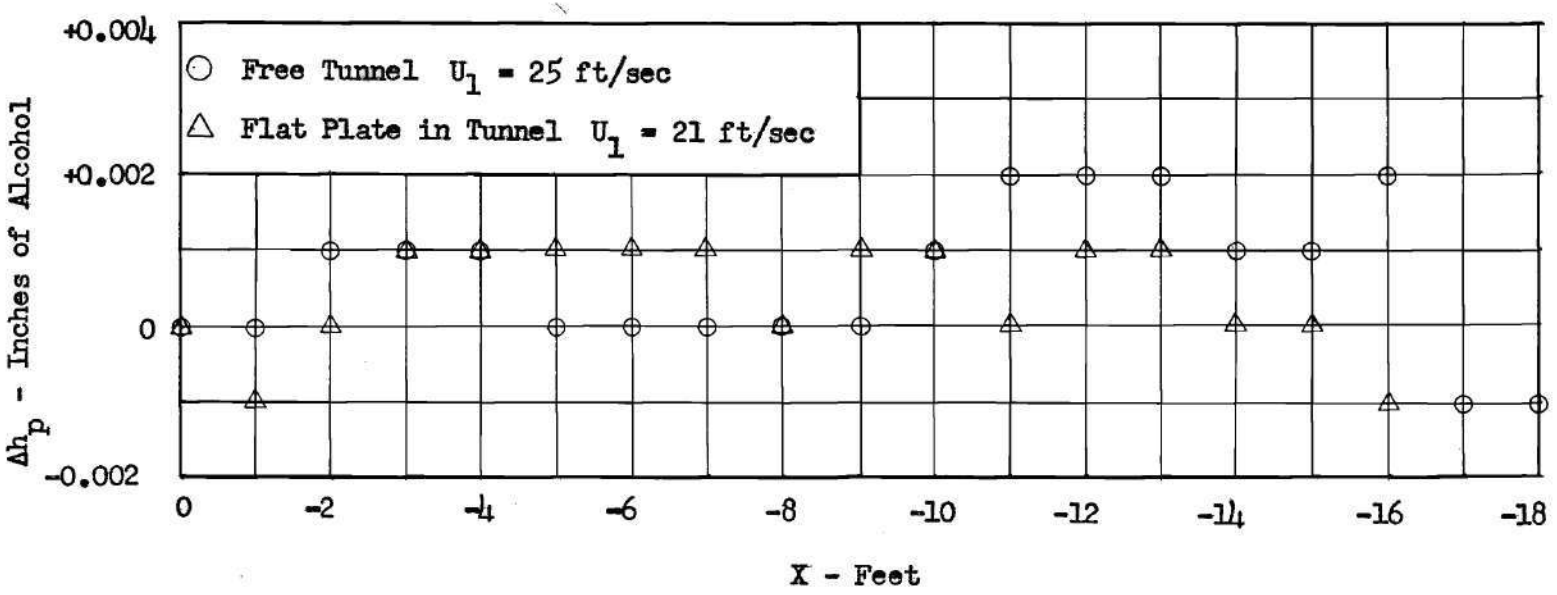

Fig. 4 Longitudinal Static Pressure Distribution

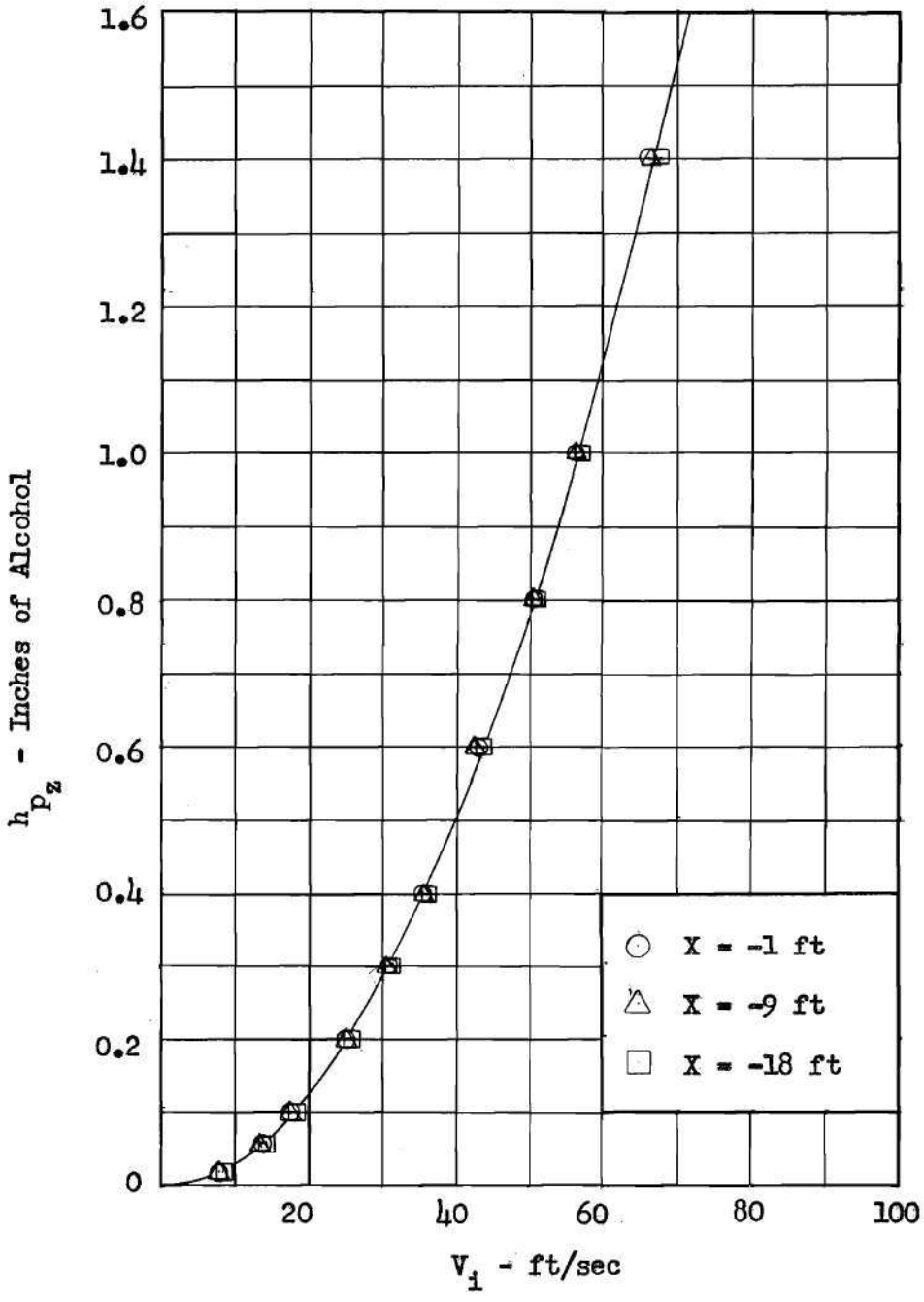

Fig. 5 Speed Calibration

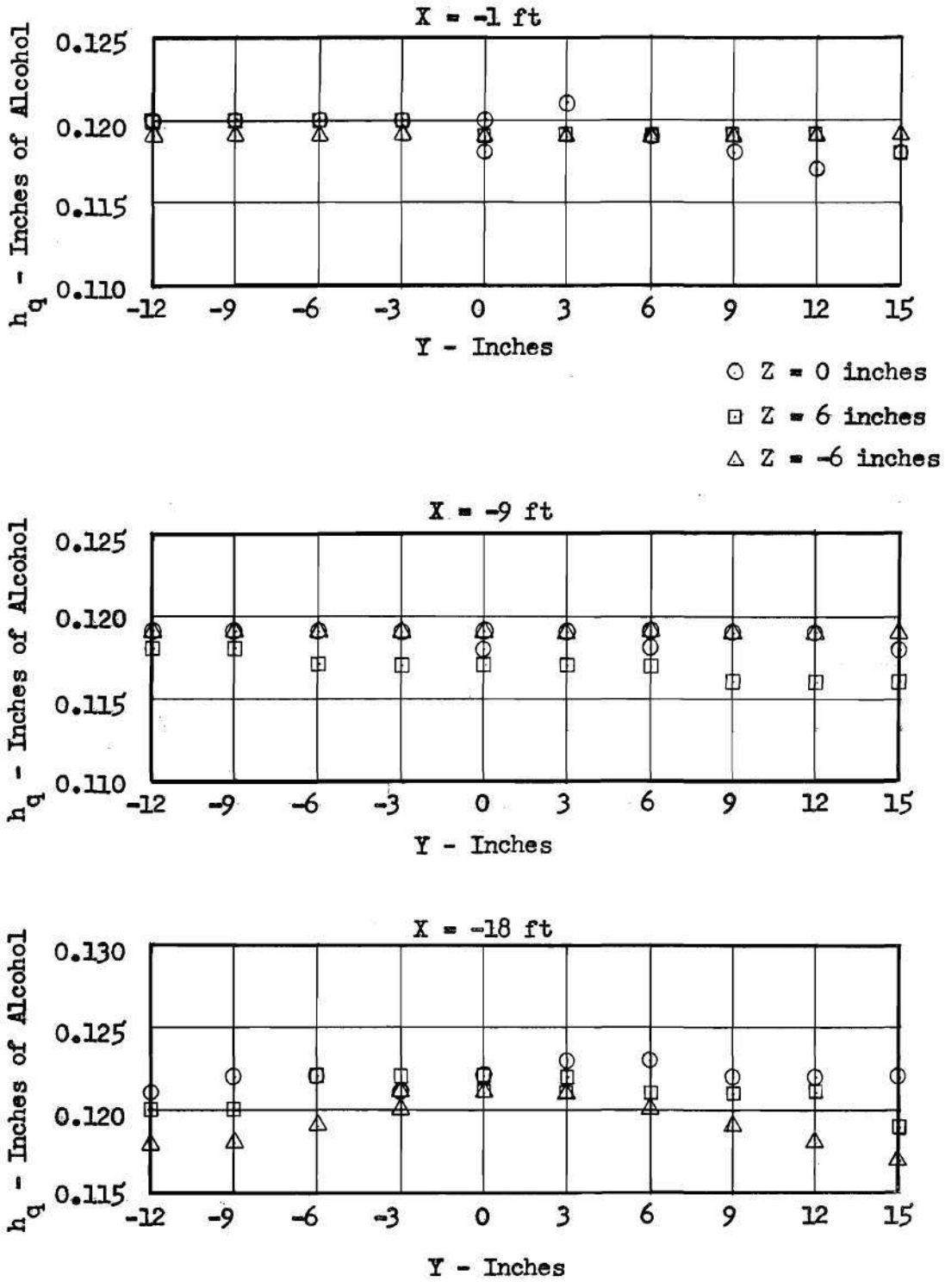

Fig. 6 Dynamic Pressure Surveys
U_1 = 21 ft/sec

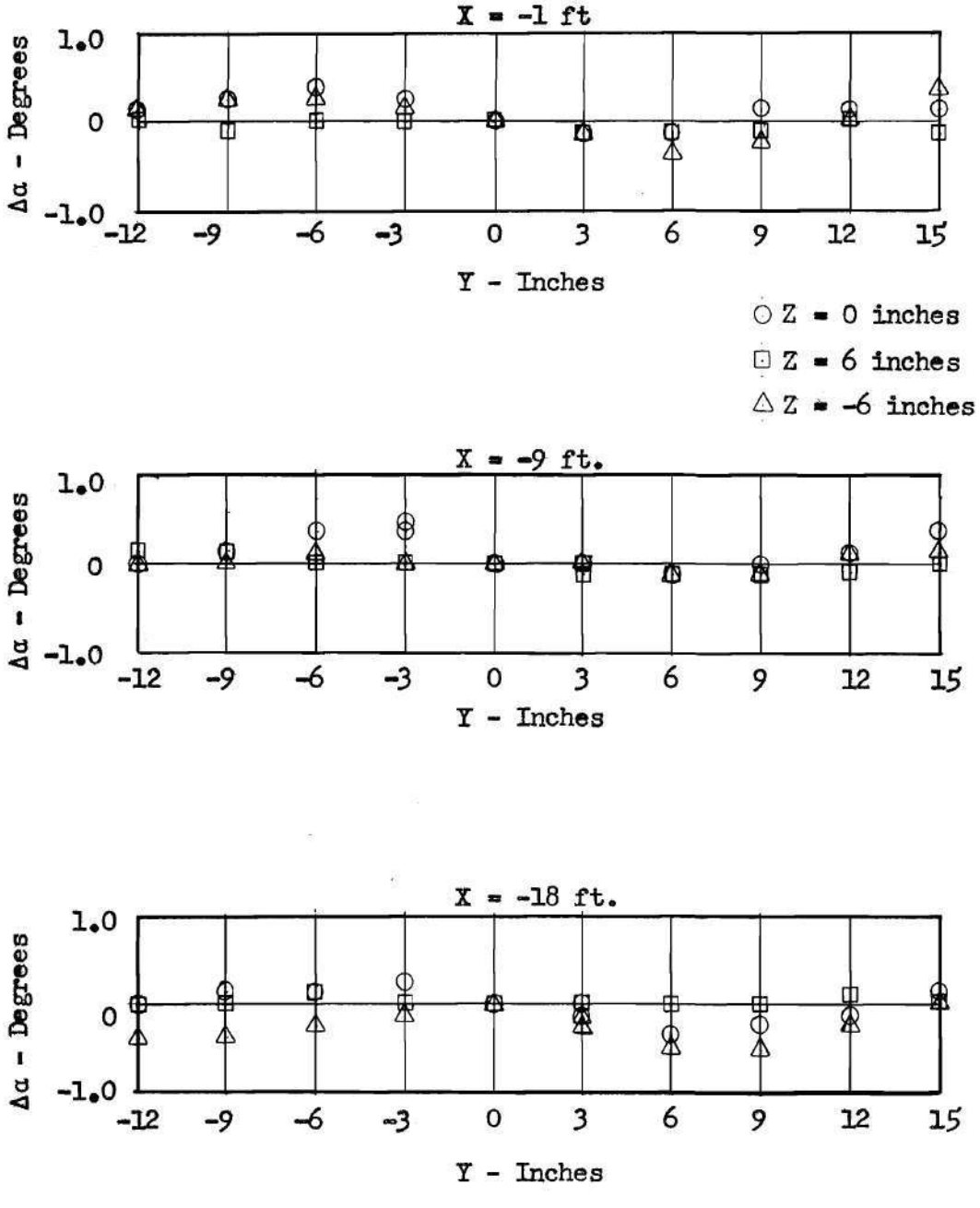

Fig. 7 Vertical Plane Angularity Deviations Referenced to Center Line Values

U_1 = 21 ft/ sec

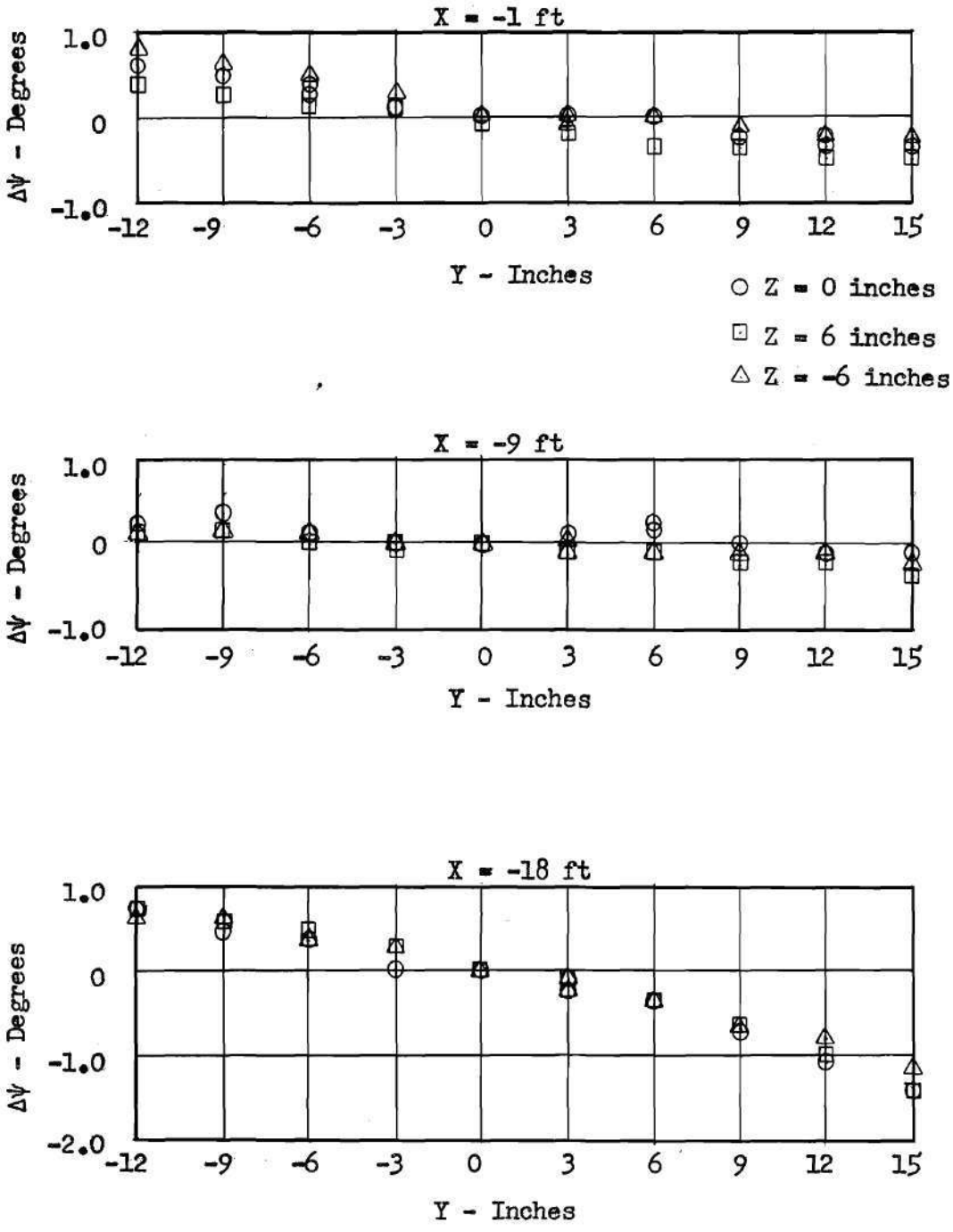

Fig. 8 Horizontal Plane Angularity Deviations Referenced to Center Line Values

U_1 = 21 ft/sec

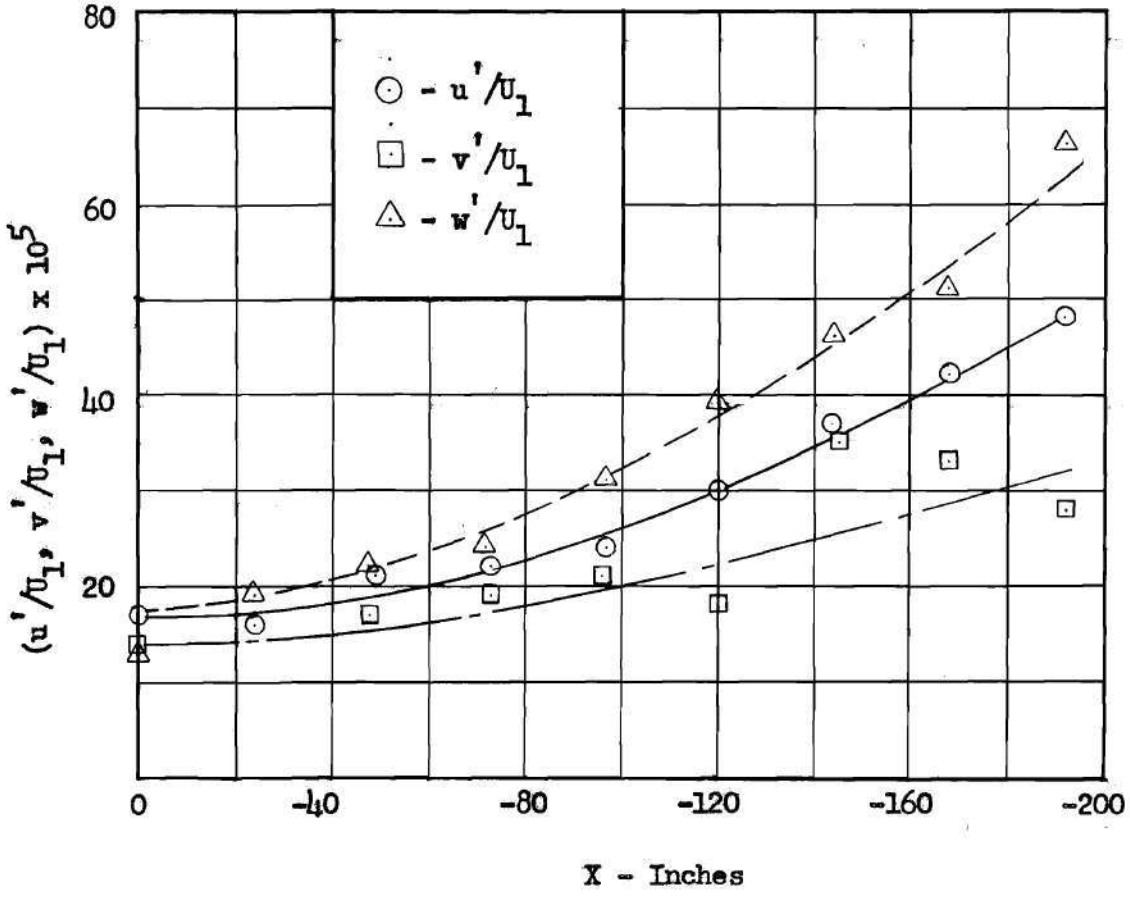

Fig. 9 Free Tunnel Turbulence Surveys Along Longitudinal Center Line

U_1 = 21 ft/sec

$\partial h_p / \partial X = 0$

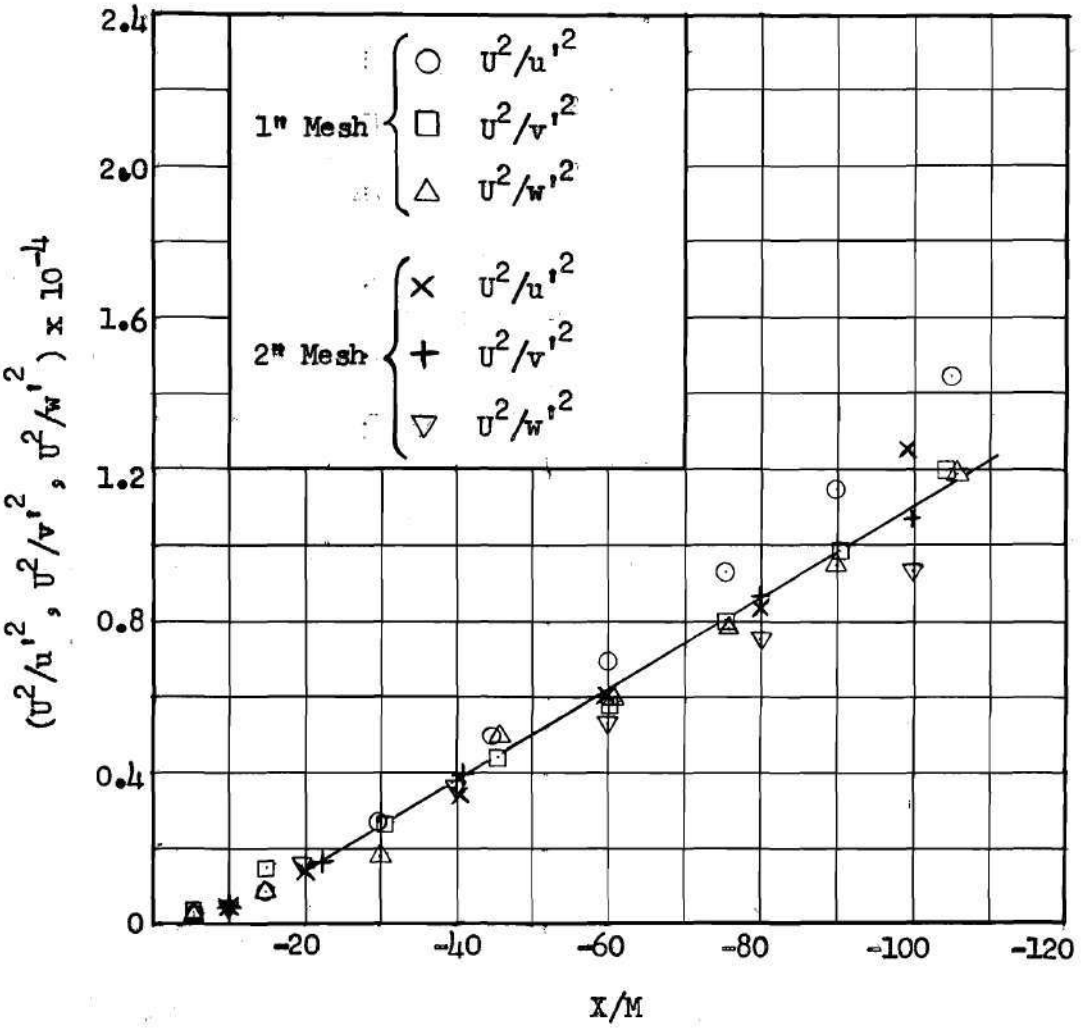

Fig. 10 Decay of Turbulence Behind 1" and 2" Square Mesh Grids

U_1 = 21 ft/sec

$\partial h_p / \partial X = 0$

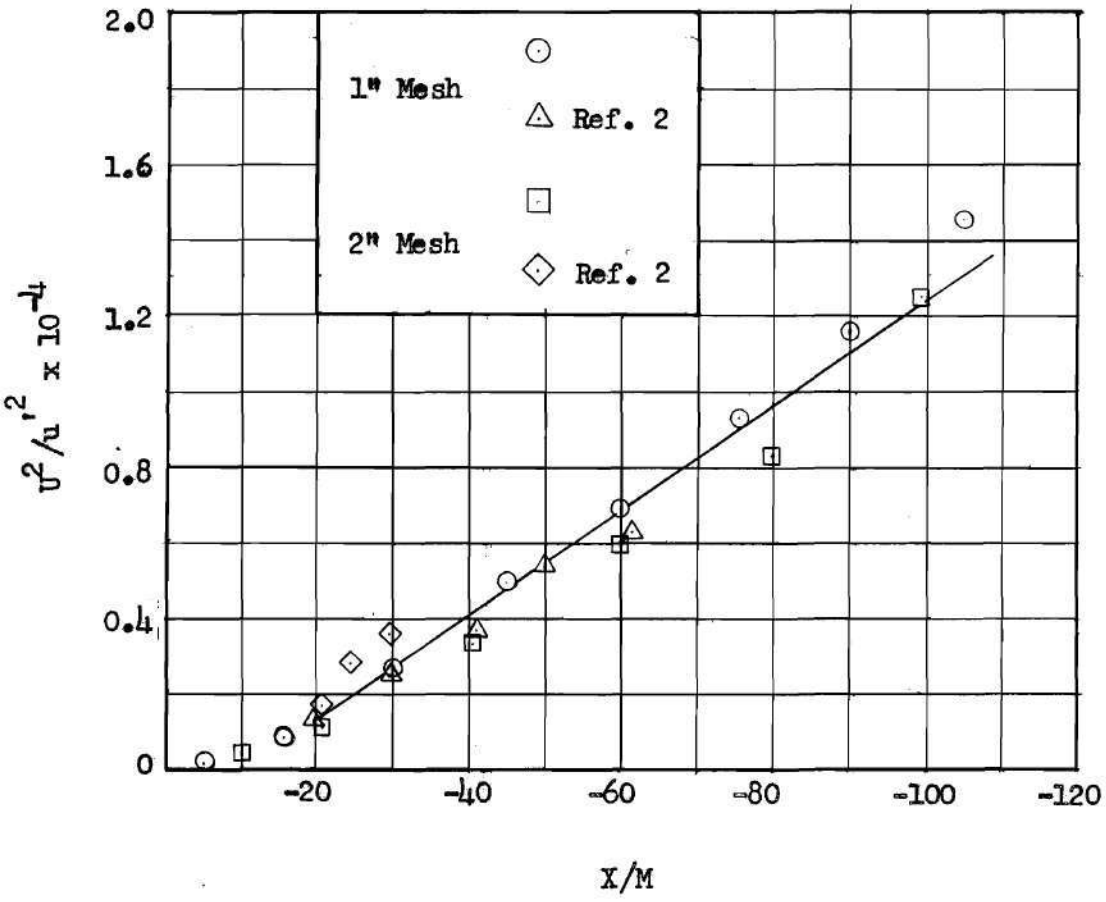

Fig. 11 Comparison of Longitudinal Turbulence Decay With Data of Reference 2 for 1" and 2" Square Mesh Grids U_1 = 21 ft/sec

$\partial h_p / \partial X = 0$

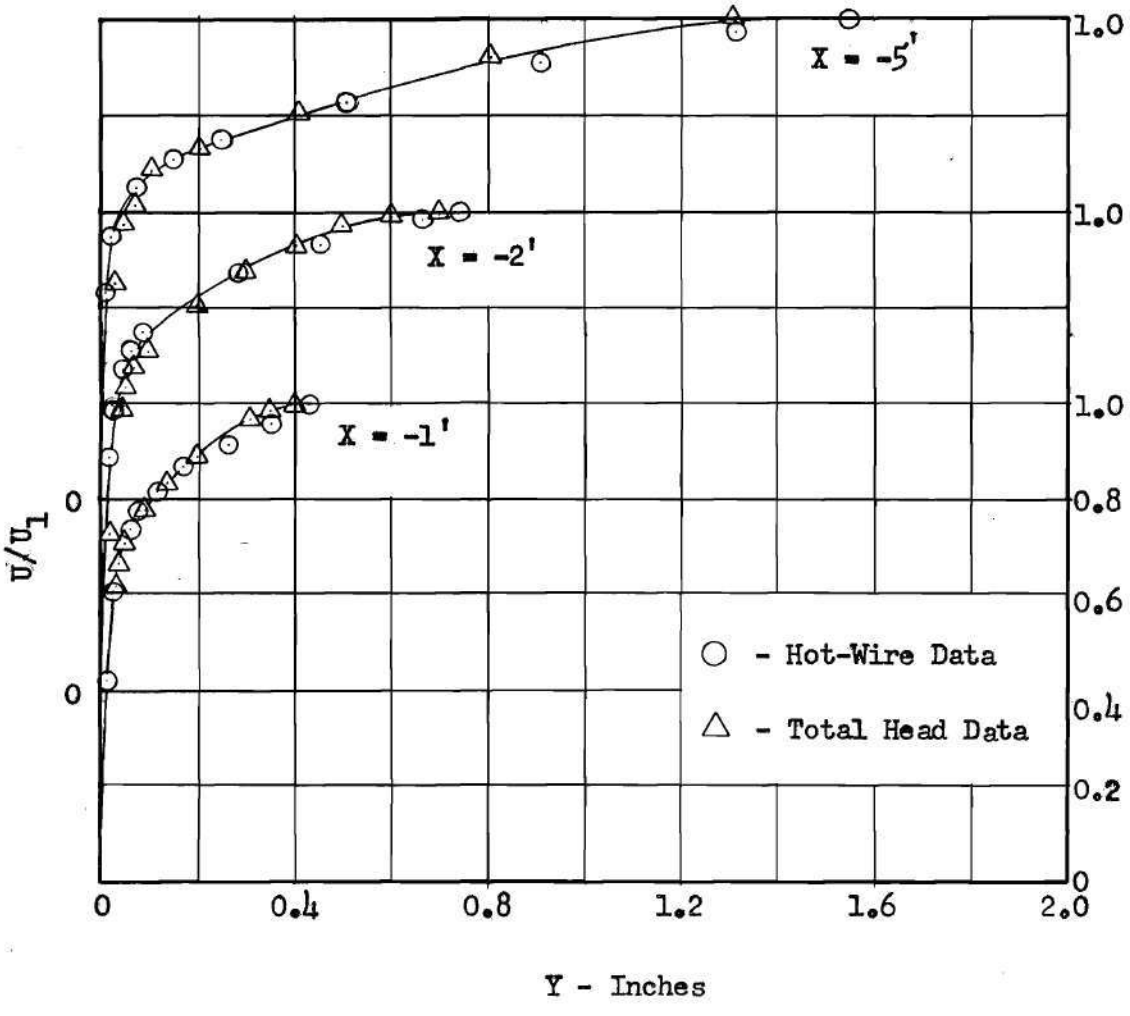

Fig. 12 Turbulent Boundary-Layer Velocity Profiles

$U_1 = 21$ ft/sec

$\partial h_p / \partial X = 0$

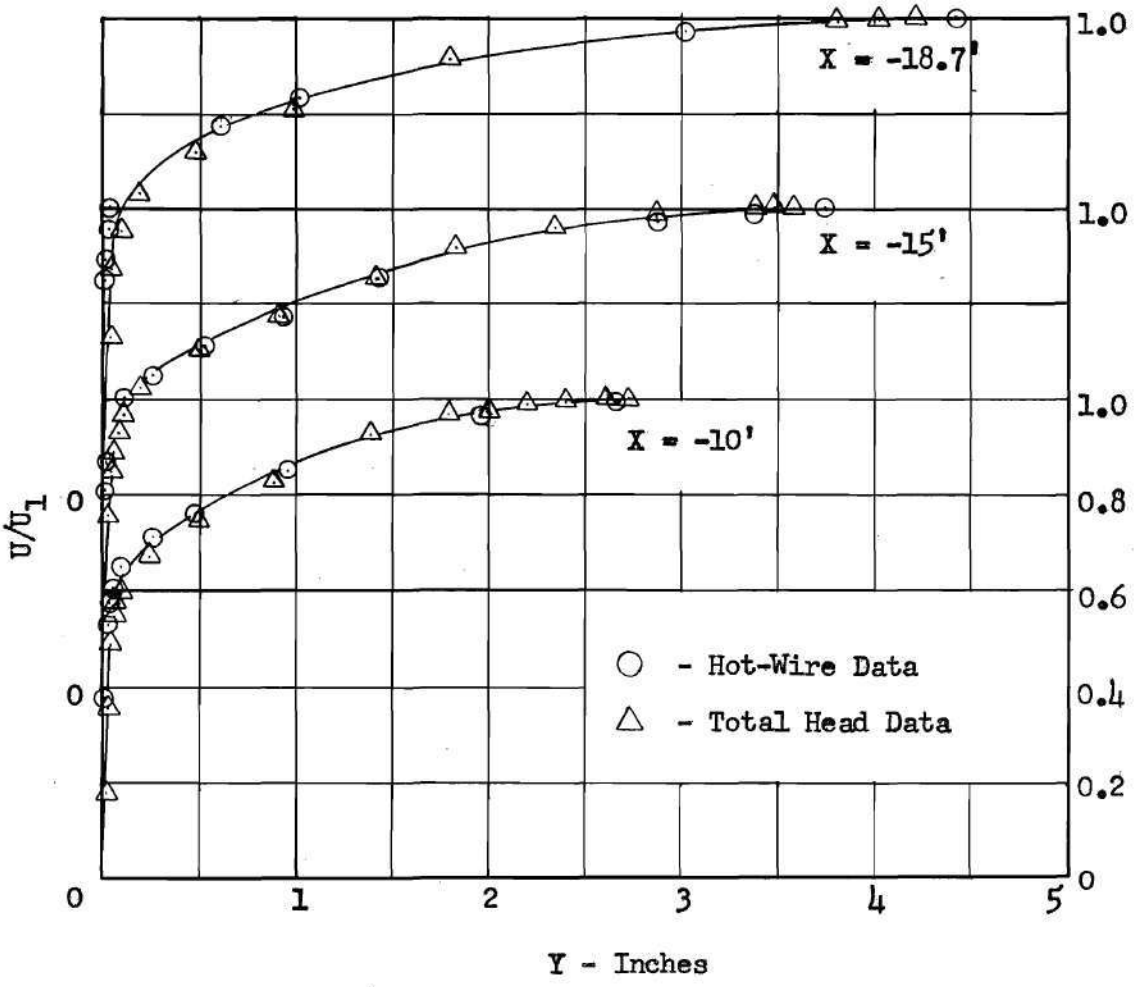

Fig. 13 Turbulent Boundary-Layer Velocity Profiles

$U_1 = 21$ ft/sec

$\partial h_p / \partial X = 0$

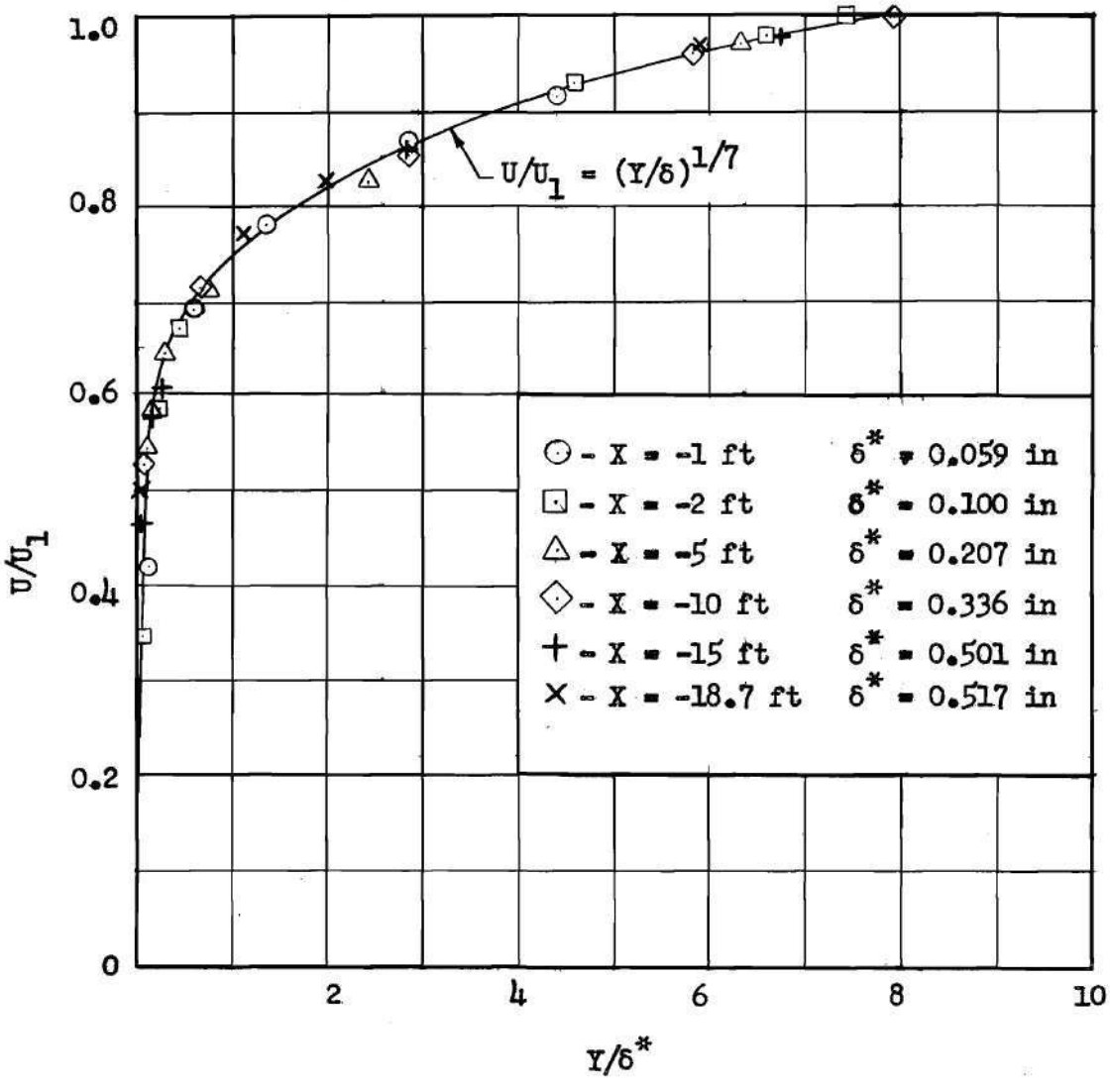

Fig. 14 Comparison of Measured Velocity Profiles With 1/7 Power Law

U_1 = 21 ft/sec

$\partial h_p / \partial X = 0$

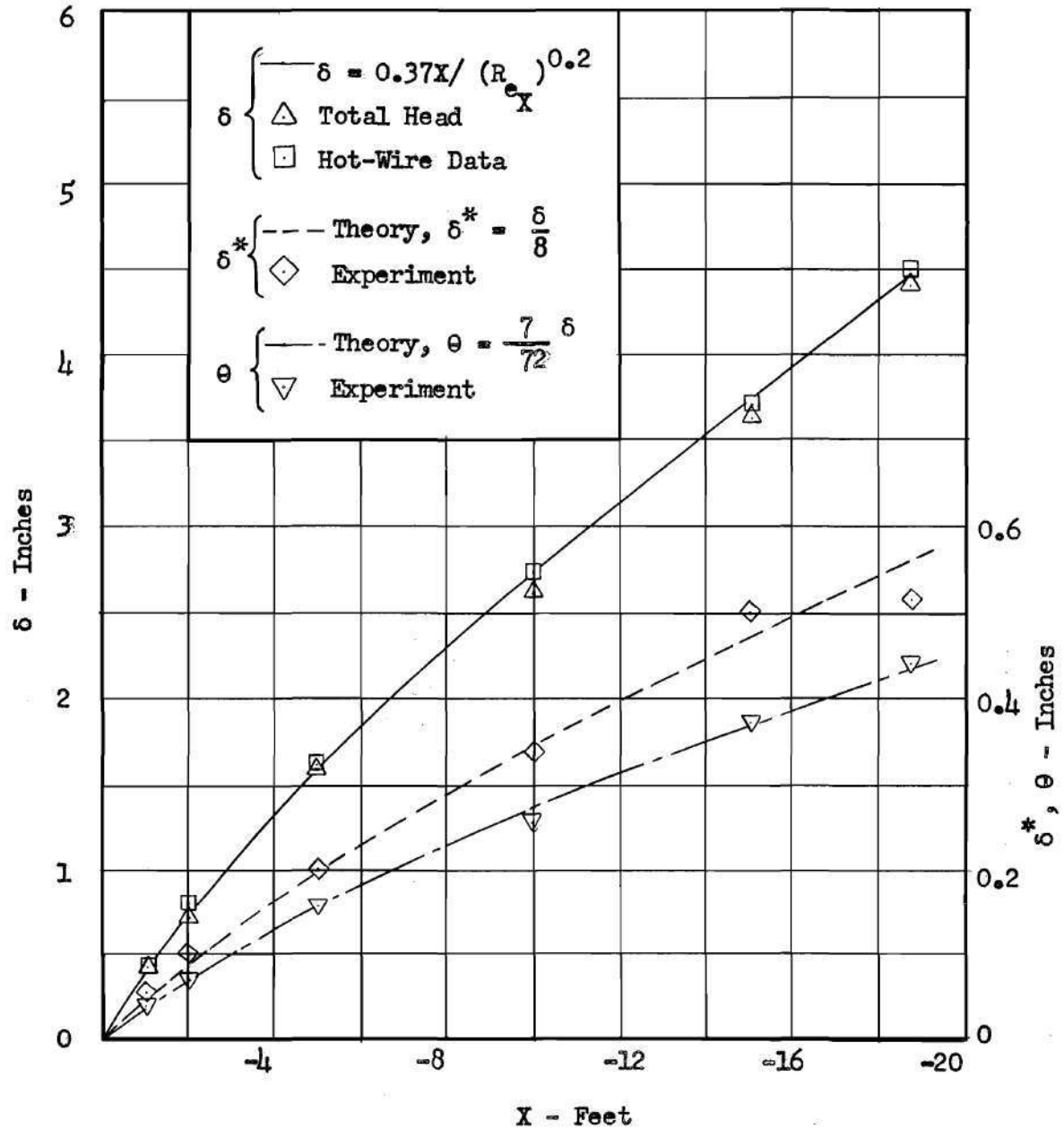

Fig. 15 Comparison of Boundary-Layer Parameters Predicted By 1/7 Power Law With Measured Data

U_1 = 21 ft/sec

$\partial h_p / \partial X = 0$

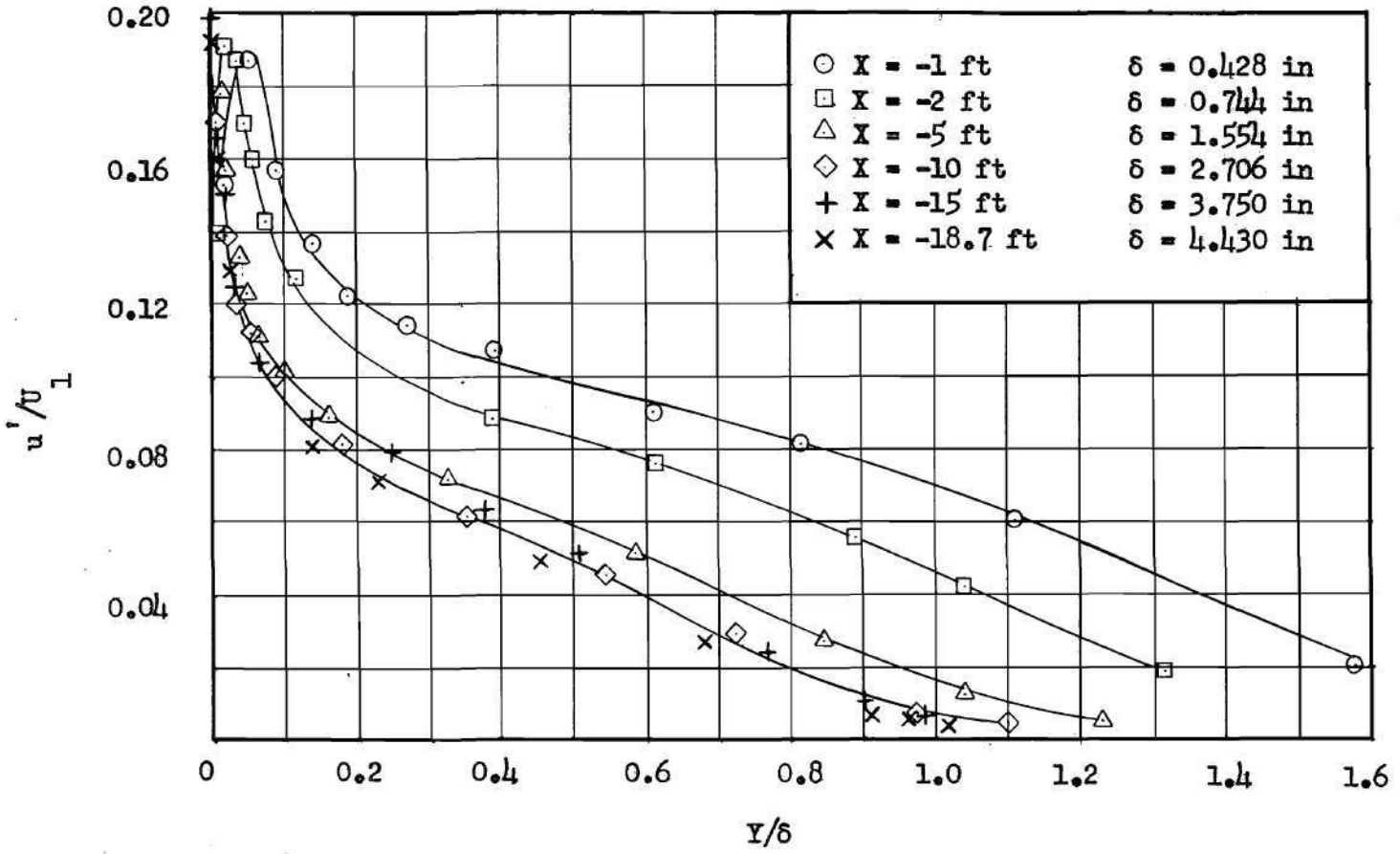

Fig. 16 Boundary-Layer Distribution of Intensity of Longitudinal Turbulence Component

U_1 = 21 ft/sec

$\partial h_p / \partial X = 0$

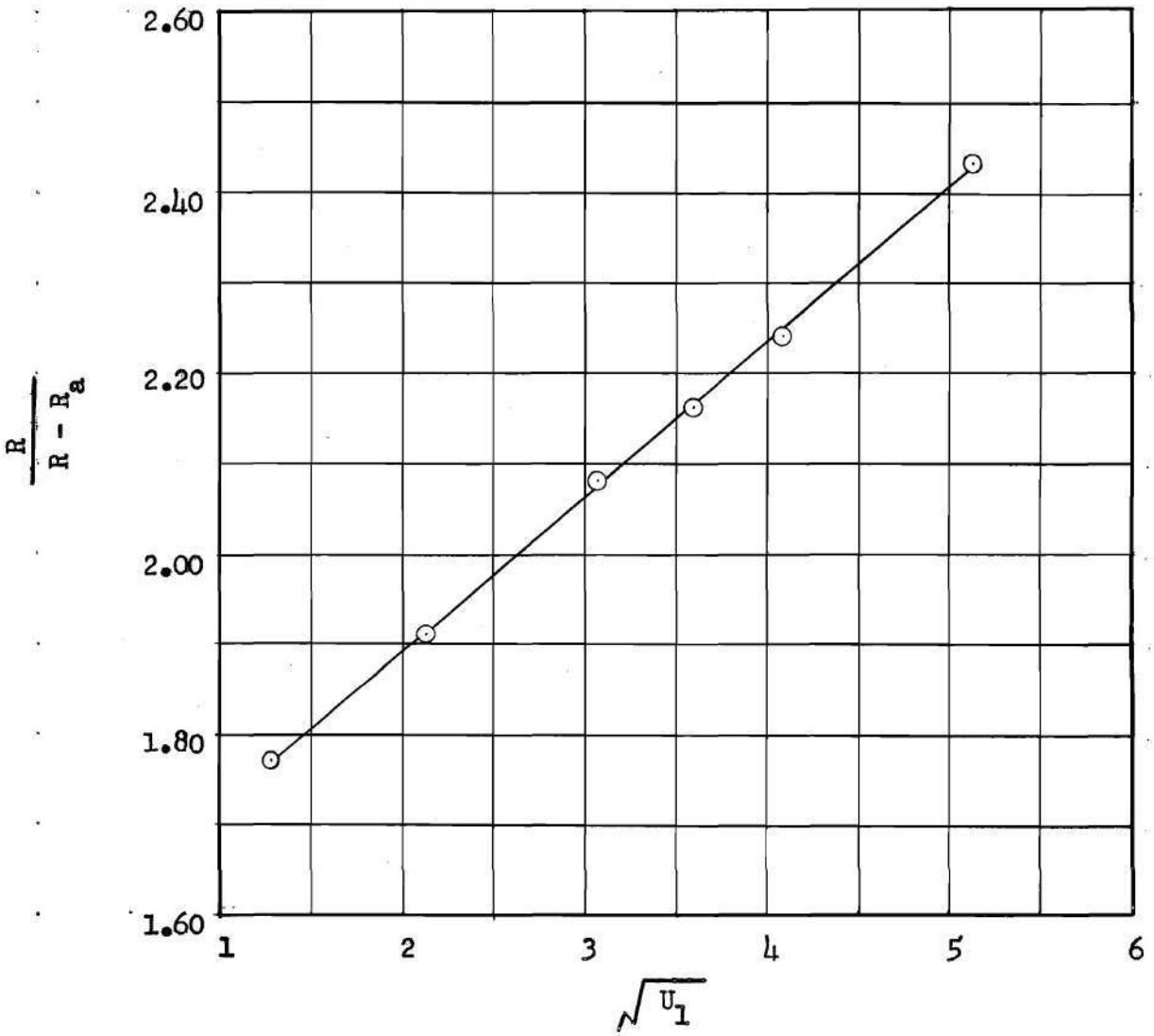

Fig. 17 Sample Calibration Curve For A Single Wire Probe

REFERENCES

1. Wharton, C. L., Jr., Part I - The Effect of Screens In a Wide-Angle Diffuser of Square Cross-Section. Part II - The Influence of the Proximity of a Wall to the Test Section Exit of a Wind Tunnel. Unpublished Master's Thesis, Georgia Institute of Technology, 1954.

2. Schubauer, G. B. and W. G. Spangenberg, Effect of Screens in Wide-Angle Diffusers. National Advisory Committee for Aeronautics, Technical Note 1610, 1948.

3. Batchelor, G. K. and A. A. Townsend, "Decay of Turbulence in the Initial Period," Proceedings of the Royal Society of London, Series A, vol. 193 (1948), pp. 539-558.

4. Pai, Shih-I, Viscous Flow Theory II - Turbulent Flow, D. Van Nostrand Co., Inc. 1957.

5. King, L. V., "On the Convection of Heat from Small Cylinders in a Stream of Fluid: Determination of the Convection Constants of Small Platinum Wires with Applications to Hot-Wire Anemometry", Philosophical Transactions of the Royal Society, London, Series A, vol. 214 (1914), pp. 373-432.

6. Schubauer, G. B. and P. S. Klebanoff, Theory and Application of Hot-Wire Instruments in the Investigation of Turbulent Boundary Layers. National Advisory Committee for Aeronautics, Wartime Report W-86, 1946.